Geochemistry Geophysics Geosystems G3
AN ELECTRONIC JOURNAL OF THE EARTH SCIENCES
Published by AGU and the Geochemical Society

Article
Volume 6, Number 10
8 October 2005
Q10002, doi:10.1029/2005GC000919
ISSN: 1525-2027

Why do kimberlites from different provinces have similar trace element patterns?

Yakov Khazan and Yuri Fialko

Institute of Geophysics and Planetary Physics, Scripps Institution of Oceanography, University of California San Diego, 9500 Gillman Drive, La Jolla, California 92093, USA (ykhazan@ucsd.edu; yfialko@ucsd.edu)

[1] Analysis of the trace element contents in kimberlites from various provinces around the world, including South Africa, India, and Yakutia (Siberia, Russia), reveals remarkable similarity of the maximum abundances. In addition, we find that abundances of the rare earth elements (REE) in the South African kimberlites are highly coherent between individual elements. We suggest that the observed similarity of the trace element patterns may result from a common physicochemical process operating in the kimberlite source region, rather than from peculiar source compositions and magmatic histories. The most likely candidates for such a process are (1) partial melting at very low melting degrees and (2) porous melt flow and diffusive exchange with the host rocks. These two processes can produce the same maximum trace element abundances and similar undersaturated patterns. We argue that the porous flow, and the associated chromatographic enrichment, is preferred because it allows high saturations at relatively large melt fractions of ~1%. Observations of enrichment of the xenolith grain rims due to an exchange with metasomatizing melts of quasi-kimberlitic composition imply that the melt percolated beyond the source region, in agreement with basic assumptions of the percolation model. We demonstrate that the saturated REE patterns are in a good agreement with the maximum observed REE abundances in kimberlites from different provinces. The theoretical patterns are independent of the melt fraction and only weakly (if at all) depend on the source modal composition. Characteristic diverging fan-like patterns of trace elements predicted by the percolation model are identified in kimberlites from South Africa. We propose that a high coherency of the REE patterns in the South African kimberlites results from a general dependence of all REE abundances on the calcium content. According to this interpretation, the overall depletion of the source rocks in REE with temperature (and depth) postulated by our model is a natural consequence of a decrease in the calcium content along the lherzolite trend.

Components: 12,543 words, 16 figures, 1 table.

Keywords: kimberlites; melt percolation; partial melting; rare earth elements.

Index Terms: 1038 Geochemistry: Mantle processes (3621); 1037 Geochemistry: Magma genesis and partial melting (3619).

Received 12 January 2005; **Revised** 8 July 2005; **Accepted** 21 July 2005; **Published** 8 October 2005.

Khazan, Y., and Y. Fialko (2005), Why do kimberlites from different provinces have similar trace element patterns?, *Geochem. Geophys. Geosyst.*, *6*, Q10002, doi:10.1029/2005GC000919.

1. Introduction

[2] Kimberlitic magmas are unique in that they originate from the greater depths than any other magma types, and are the major source of mantle xenoliths providing direct information about the composition and thermodynamic conditions in the shallow upper mantle. This, along with the diamondiferous nature of some kimberlites, resulted in intensive geological, petrological and geochemical studies of kimberlites [e.g., *Dawson*, 1980; *Mitchell*, 1986; *Ukhanov et al.*, 1988; *Vladimirov et al.*, 1990; *Wyllie*, 1995; *Mitchell*, 1995]. One of the distinctive features of kimberlites is their enrich-

ment in incompatible elements relative to most other magma types, as well as to a "primitive" mantle. In particular, the chondrite-normalized abundances of light rare earth elements (LREE) are typically of the order of 10^3 [e.g., *Dawson*, 1980; *Mitchell*, 1986; *le Roex et al.*, 2003; *Golubeva et al.*, 2003; *Chalapathi Rao et al.*, 2004]. This has led to hypotheses of the kimberlite production by either extremely low degrees of melting of a common upper mantle peridotite [*Dawson*, 1971; *Wyllie*, 1980], or melting of a peculiar source region that experienced a long and complex history (e.g., the "depletion, enrichment and melting" sequence of *Tainton and McKenzie* [1994]). According to single-stage melting scenarios, the kimberlitic magmas might result from very low degrees of melting of a garnet lherzolite mineral assemblage under hydrous and/or CO_2 saturated conditions [*Dawson*, 1971; *Eggler and Wendlandt*, 1979; *Wyllie*, 1980; *Eggler*, 1989]. However, in order to explain the observed LREE enrichments the melting degree needs to be less than 0.1% to account for the thousand-fold enrichment in LREE relative to a primitive upper mantle. Although an interconnected melt network can in principle form even for infinitesimal melt fractions, provided that the dihedral angle is less than 60° [e.g., *Laporte and Provost*, 2000], so that it might be possible to extract the melt given sufficiently low melt viscosity [e.g., *McKenzie*, 1989], available laboratory data indicate that the porous flow may not be very efficient at low melt fractions. For example, measurements of permeability of synthetic quarzites having porosities as low as 0.6% suggest a cubic dependence of permeability on porosity, in contrast with the theoretically predicted quadratic dependence [*Wark and Watson*, 1998; *Liang et al.*, 2001]. If so, for reasonable parameters (e.g., the average grain size of the order of 1 mm, the dynamic viscosity of kimberlitic melts of 0.1 Pa s, and the density contrast between the melt and the host rock of 1–10%), porosities of the order of 10^{-3} imply the velocity of melt segregation of the order of 0.3–3 mm/yr, perhaps too low for an efficient transport of melt over the timescales of the order of 10^6 years characteristic for the transient magmatic activity in a kimberlite field *Heaman et al.* [2003a, 2003b], and typical of a plume-induced thermal perturbation in the upper mantle [*Crough et al.*, 1981; *White and McKenzie*, 1989; *Fialko and Rubin*, 1999]. In addition, *Faul* [1997] argued that a substantial fraction of melt may reside in flat pockets at the grain sides rather than in the triple junction tubules, so that the permeability may remain low until the pockets interconnect at melt fractions of about 2–3%. These arguments imply that melt migration via porous flow may be significantly impeded at the low melt fractions required to explain the geochemistry of kimberlites according to hypotheses of single-stage melting of a "common" mantle source.

[3] The alternative multistage melting models explain the observed geochemical signatures of kimberlites in terms of a source composition that is fractionated relative to a primitive upper mantle. For example, *Tainton and McKenzie* [1994] suggested a sequence of events that could produce magmas of kimberlitic composition from a mid-ocean ridge basalt (MORB) source. According to their model, the first stage is a strong depletion of a MORB source by extraction of ~20% melt in the garnet stability field, followed by a metasomatism of the depleted source by an addition of 5–10% of magmas produced by 0.3–5% melting of the MORB source, and finally 0.3–0.4% melting of the metasomatized source to produce liquids with kimberlitic REE abundances. Similarly, *le Roex et al.* [2003] explained the observed trace element ratios of the so-called Group I kimberlites by a 0.4–1.5% melting of a metasomatized garnet lherzolite source in the sub-lithospheric mantle; the postulated metasomatic event is assumed to produce a 2 to 5-fold enrichment in LREE and approximately a 3-fold depletion in heavy rare earth elements (HREE) compared to a primitive mantle, thereby not requiring very low degrees of melting. *Ringwood et al.* [1992] and *Kesson et al.* [1992] proposed that the kimberlitic magmas originate from sources in the transition zone that were fertilized by melts derived from the subducted oceanic lithosphere, on the basis of isotopic and trace element similarities between Group I kimberlites and ocean island basalts (OIB).

[4] Figure 1 shows the observed range of the trace element (REE as well as Rb, Ba, Th, Ta, Nb, Sr, Zr, Hf) contents from the South African, Yakutian (Siberia, Russia), and Indian kimberlite provinces. As one can see from Figure 1, the variability in the REE abundances between different provinces is smaller than the variability within a single province. Furthermore, the maximum observed values of the REE enrichment are nearly identical in different provinces. These observations are not easily explained by the existing theories of the origin of kimberlites. In particular, the coincidence in the maximum REE abundances in different settings would imply the same minimum degree of melting of the kimberlite source according to a single-stage melting hypothesis, and the same sequence of magmatic and metasomatic events according to a mul-

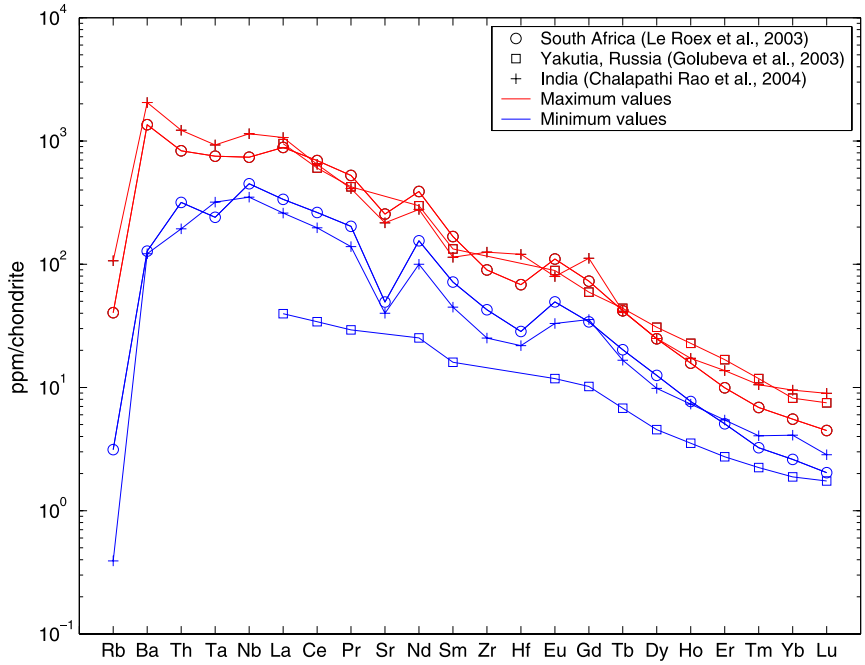

Figure 1. Trace element patterns observed in the South African (23 samples [*le Roex et al.*, 2003]), Yakutian (40 samples [*Golubeva et al.*, 2003]), and Indian (54 samples [*Chalapathi Rao et al.*, 2004]) kimberlites. Solid lines denote the maximum, and dashed lines denote the minimum trace element abundances in kimberlites from South Africa (circles), Yakutia (squares), and India (crosses). Note that for the Yakutia province only REE data are available.

tistage melting hypothesis. If so, mechanisms that might control such a repeatable and consistent melting process themselves remain a major mystery.

[5] In this paper we consider an alternative model to explain the observed geochemical features of kimberlitic magmas from various settings around the world. The model explores the geochemical consequences of percolation of melt through the host rocks, i.e., a process that is a fundamental and integral part of in situ melting and subsequent melt segregation [e.g., *McKenzie*, 1985; *Kelemen et al.*, 1997; *Kohlstedt et al.*, 2000]. We shall demonstrate that the geochemical interaction between the melt and the ambient rocks, also referred to as the chromatographic column fractionation [*Korzhinskii*, 1970; *Hofmann*, 1972; *Navon and Stolper*, 1987], or percolative crystallization [*Harte et al.*, 1993; *Burgess and Harte*, 2004], is alone able to account for the observed values of the REE abundances in kimberlites from different provinces, without any special assumptions about the degree of melting, and the initial source composition. A well-established consequence of a chemical exchange between the melt and the host rocks is that the melt emerging at the top of the chromatographic column may have a composition typical of an infinitesimal degree of melting, even though the melt fraction at the base of the column is not necessarily small [*Korzhinskii*, 1970; *Hofmann*, 1972; *Navon and Stolper*, 1987]. Therefore the metasomatic alteration accompanying the mobilization and evacuation of melt from the source region may reconcile relatively large degrees of melting (and, correspondingly, an efficient melt extraction) with an extreme REE enrichment of kimberlites. The effects of mantle metasomatism are well documented by studies of mantle xenoliths from regions associated with kimberlitic magmas [e.g., *Harte*, 1987; *Harte et al.*, 1993; *McKenzie and O'Nions*, 1991; *Grégoire et al.*, 2000, 2003; *Dawson*, 2002; *Ionov et al.*, 2002b; *le Roex et al.*, 2003; *Burgess and Harte*, 2004]. Furthermore, the geochemical characteristics of metasomatized peridotitic xenoliths are often interpreted as requiring metasomatic fluids that are similar in composition to kimberlitic melts [*Menzies et al.*, 1987; *Erlank et al.*, 1987; *Harte et al.*, 1993; *Grégoire et al.*, 2003; *Ionov et al.*, 2002b; *le Roex et al.*, 2003; *Burgess and Harte*, 2004]. At the same time, the observed enrichments in the grain rims indicate that the melts percolated beyond the regions from which they were derived. Here we show that the chromatographic model obviates the need for any peculiar composition of the source region. In particular, we demonstrate that the observed trace element signatures of kimberlites are consistent with

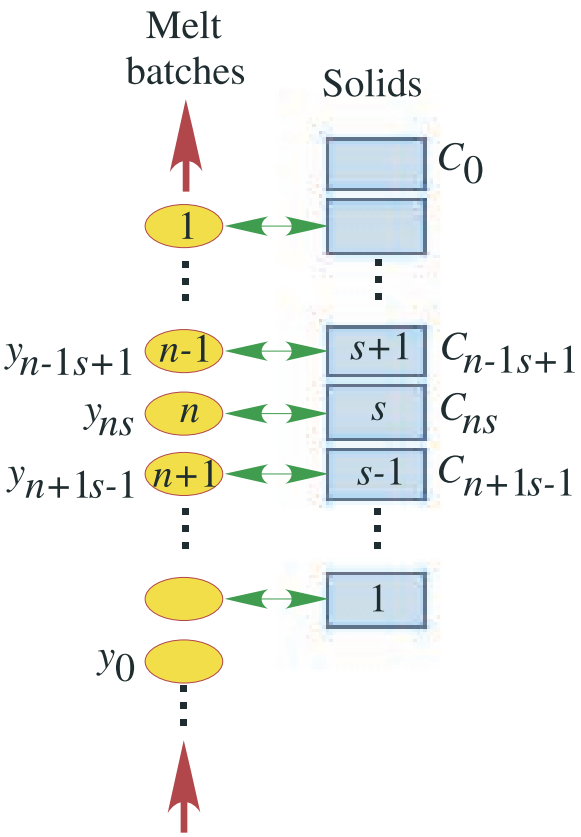

Figure 2. Schematic representation of chemical interactions during the melt diffusion. Melt batches denoted by ellipses (1, .., *n*, ..) propagate through a solid matrix (rectangles 1, .., *s*, ..) and undergo a diffusive exchange symbolically indicated by the green arrows. The initial abundances of trace element in the melt is y_0. The initial abundances in all the solids are C_0. Abundances of a trace element in a melt batch y_{jk} and in a solid C_{jk} correspond to a full equilibrium between the *j*-th batch of melt with the *k*-th volume of solid. For example, in the result of equilibration of the *n*-th melt batch with the *s*-th volume of solid the abundances change from y_{ns-1} to y_{ns} and from C_{n-1s} to C_{ns} in the melt and solid, respectively.

the kimberlite origin from a "normal" (i.e., unmetasomatized) upper mantle peridotite. We also show that the saturated trace elements abundances in a percolating melt or in an infinitesimal melt only weakly if at all depend on a modal composition of the source rocks, as well as on the melt fraction. The inferred universal signatures of the saturated abundances of trace elements may explain similar trace element contents observed in kimberlites from different provinces worldwide.

2. Mathematical Formulation

[6] Melt percolation through a solid matrix is a complex physicochemical process that involves melting, crystallization, chemical interactions, and diffusive exchange between the melt and the solid matrix. Some quantitative aspects of the evolution of trace elements during percolation were discussed, e.g., by *Navon and Stolper* [1987] and *Maaløe* [1995], but a complete description of the continuously evolving melt-solid phase relations that accompany in situ melt percolation [*Harte et al.*, 1993; *Burgess and Harte*, 2004] is not yet available. We begin by developing a simple formalism to describe the evolution of a trace element composition of melt that propagates (e.g., via porous flow) through a solid matrix in a style similar to the "chromatographic column" model of *Korzhinskii* [1970], *Hofmann* [1972], and *Navon and Stolper* [1987].

[7] Let V be the melt velocity, and L be the overall distance of melt migration. If the melt and solid phases are out of the chemical equilibrium, the diffusive exchange between the phases will occur with the characteristic timescale $\tau = a^2/\pi\kappa$, where κ is the chemical diffusivity, and a is the characteristic distance between melt inclusions (likely of the order of the grain size). We consider the evolution of a discrete batch of melt which size d is much smaller than the total propagation distance L, but larger than the distance $V\tau$ corresponding to a full chemical equilibration, $V\tau \leq d \ll L$. To gain a quantitative insight into the chemical evolution of the system, we make the following simplifications. First, we assume that the mass of melt is constant, and proportions of the solid phases do not change during the melt-solid interaction, so that the chemical effects of crystallization and melting are assumed to be negligible. Second, we ignore the effects of diffusion. The latter assumption has two implications: (1) the metasomatic reactions are considered to be a sequence of equilibrium steps such that at each step we assume an equilibrium partitioning of trace elements between the melt batch and the solid rock and (2) the effects of dispersion in the column are neglected. Our model treats interactions between the melt and solid as a series of discrete events: melt is brought into a contact with a "fresh" host rock; trace elements are distributed between the melt and the solid until an equilibrium is achieved; the melt moves further, and the process repeats itself (see Figure 2). Every following batch that tracks the same trajectory interacts with the solid that has been partly depleted (or enriched) in the result of equilibration with the preceding melt batches.

Hereinafter we will not make a distinction between the enrichment and depletion, and use the term "enrichment" regardless of whether the particular element abundance increases or decreases. For a large enough number of the enrichment cycles, and a given initial composition of the solid volumes that interact with melt, the element abundance in the melt asymptotically approaches an equilibrium with the initial composition of the host rock. We shall refer to such melt as the "saturated" one; any melt that has not yet achieved the corresponding composition will be referred to as "unsaturated". Conceptually, our analysis is similar to that of *Navon and Stolper* [1987]. It differs in that we will be able to reduce the problem to a closed algebraic solution, rather than a system of differential equations, thereby allowing for a robust analytic insight. Consider a batch of a melt having mass m that comes in contact with a garnet lherzolite host having mass M and consisting of olivine (*ol*), orthopyroxene (*opx*), clinopyroxene (*cpx*) and garnet (*gt*). The masses of the mineral phases and their relative abundances are M_i ($\Sigma M_i = M$) and $x_i = M_i/M$, respectively (i = *ol*, *opx*, *cpx*, *gt*). The ratio $\phi = m/M$ represents the melt fraction.

[8] Let n be a number of the current melt batch. While the first batch propagates through the solid matrix it percolates subsequently through solid volumes numbered $s = 1, 2, \ldots$. The subsequent batches flow through the same solid as illustrated in Figure 2. Also, let y_{ns} denote the trace element abundance in the n-th melt batch after it experienced the diffusive equilibration with the first s solid volumes, and C^i_{ns} denote the element abundance in the i-th modal mineral of the s-th solid after an interaction with n melt batches. Then due to a diffusive exchange of the n-th melt batch with s-th solid, a trace element content changes from my_{ns-1} to my_{ns}, and from $\Sigma M_i C^i_{n-1s}$ to $\Sigma M_i C_{ns}$ in the melt batch and solid, respectively. The diffusive exchange does not change the overall element content. The conservation of mass gives rise to the following recurrent equation,

$$\phi y_{ns} + \Sigma_i x_i C^i_{ns} = \phi y_{ns-1} + \Sigma_i x_i C^i_{n-1s}. \quad (1)$$

In equation (1), summation is performed over the modal minerals. The initial abundances in the solid are assumed to be the same everywhere along the melt propagation path, such that

$$C^i_{1s} = C^i_0. \quad (2)$$

If the diffusive equilibration between the melt and the solid is complete, then the abundances in the solid can be expressed through those in the melt,

$$C^i_{ns} = D_i y_{ns}, n > 1, \quad (3)$$

where D_i is the partition coefficient governing the element distribution between the mode i and the melt. From equations (1) to (3), one obtains

$$y_{1s}(\phi + D) = \phi y_{1s-1} + C_0, \quad (4)$$

$$y_{ns}(\phi + D) = \phi y_{ns-1} + D y_{n-1s}, n > 1, \quad (5)$$

where

$$D = \Sigma_i x_i D_i \quad (6)$$

is the bulk partition coefficient, and C_0 is the initial whole rock abundance of an element in the solid

$$C_0 = \Sigma_i x_i C_{i0}. \quad (7)$$

Equations (4) and (5) can be solved analytically (see Appendix A) to yield

$$y_{ns} = \frac{C_0}{D} + q^s \left(y_0 - \frac{C_0}{D} \right) B_{ns}, \quad (8)$$

where q is the quotient of the geometric progression series,

$$q = \frac{1}{1 + D/\phi}, \quad (9)$$

y_0 is the initial element abundance in the melt, and B_{ns} are the numeric coefficients defined in Appendix A. The quotient q is strictly less than unity (equation (9)). Even though the factors B_{ns} increase with s, the product $q^s B_{ns}$ monotonically decreases from unity to zero as s increases from zero to infinity. Therefore the second term on the right-hand side of equation (8) progressively decays with an increasing number of interactions experienced by the melt batch. In this limit, equation (8) gives rise to a well-known result,

$$y_{sat} = \frac{C_0}{D}, \quad (10)$$

i.e., at full saturation the abundance of a trace element is controlled by an equilibrium between the melt and the initial host rock composition [e.g., *Navon and Stolper*, 1987]. The key point is that the final abundance y_{sat} does not depend upon the melt

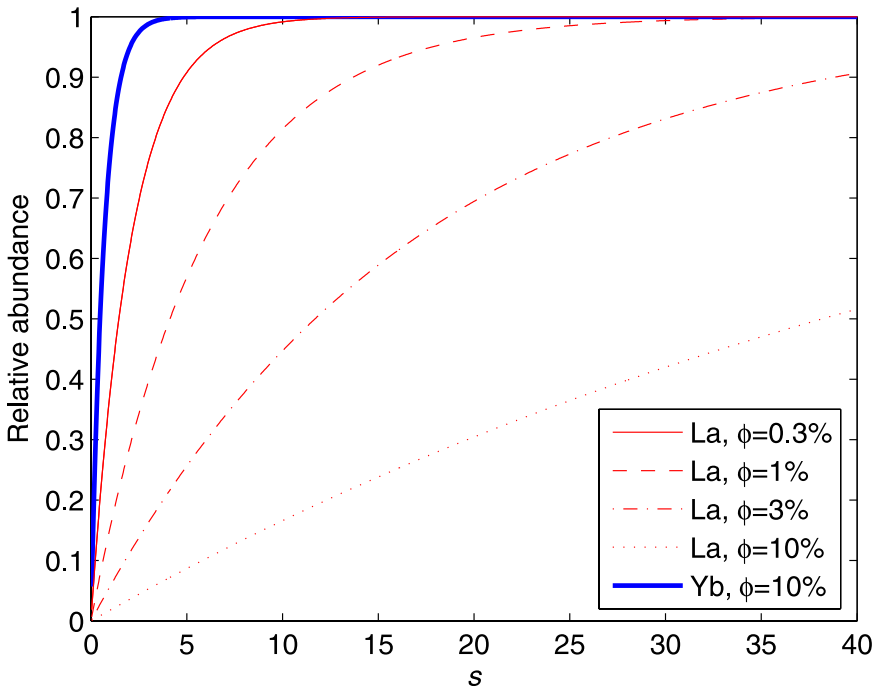

Figure 3. Rate of melt saturation in light and heavy REE. Thin curves show the dependence of La abundance in melt normalized by the abundance at full saturation versus the number of enrichment cycles, s, and melt fraction, ϕ. The heavy curve shows the relative abundance of Yb at a melt fraction of 10%.

fraction, and the melt can become highly enriched even if the melt fraction is not small.

[9] The number of enrichment cycles necessary to reach saturation strongly depends on the ratio D/ϕ. For incompatible elements and/or large melt fractions ($D/\phi \ll 1$), the quotient q (see equation (9)) is close to unity and the convergence of the geometric series (equation (8)) is slow. For compatible elements and/or small melt fractions the quotient q is small and the convergence is very rapid. This behavior is illustrated in Figure 3, which shows that HREE (e.g., Yb) abundance reaches essentially a full saturation in just a few cycles of enrichment even at melt fractions as high as 10%. This means that in general the HREE abundances in the percolating melt retain "memory" of the very last acts of enrichment only. In contrast, LREE saturate rapidly at low melt fractions (<0.3%), but require multiple cycles of enrichment to reach full saturation if the melt fraction is in excess of approximately 1%. This difference in the saturation rates implies a characteristic variation of the trace element ratios in a percolating melt. In Figure 4 we compare the behavior of Ce and Dy versus Sm. Results shown in Figure 4 correspond to a $\phi_0 = 3\%$ melt percolating through the host rocks of a constant composition. All the abundances were calculated for the first batch ($n = 1$) and normalized to their maximum values. For example, the predicted abundance of cerium is

$$\frac{Ce}{Ce_{\max}} = 1 + q_{Ce}^{s}\left(\frac{D_{Ce}}{\phi_0 + D_{Ce}(1-\phi_0)} - 1\right), \qquad (11)$$

where D_{Ce} describes the partition of cerium between the melt and the solid rock with the modal composition proposed by *Dawson* [1980], $x_{ol} = 0.66$, $x_{opx} = 0.25$, $x_{cpx} = 0.03$, $x_{gt} = 0.06$, and q_{Ce} can be found using equation (9). The abundances of other elements depend on the number of enrichment cycles in a similar way. A composition of a percolating melt evolves along the curves shown in Figure 4 from left to right. A characteristic concave shape of Ce vs. Sm curve, and a convex shape or Dy vs. Sm curve are due to differences in the rate of melt saturation with trace elements of different compatibility: the most compatible Dy saturates first, and is followed by a less compatible Sm, and an incompatible Ce. Figure 4 also shows compositions resulting from different degrees of melting of the same rock. In this case the abundance y of an element normalized by its maximum value $y_{\max}$ is given by

$$\frac{y}{y_{\max}} = \frac{D}{\phi + D(1-\phi)}. \qquad (12)$$

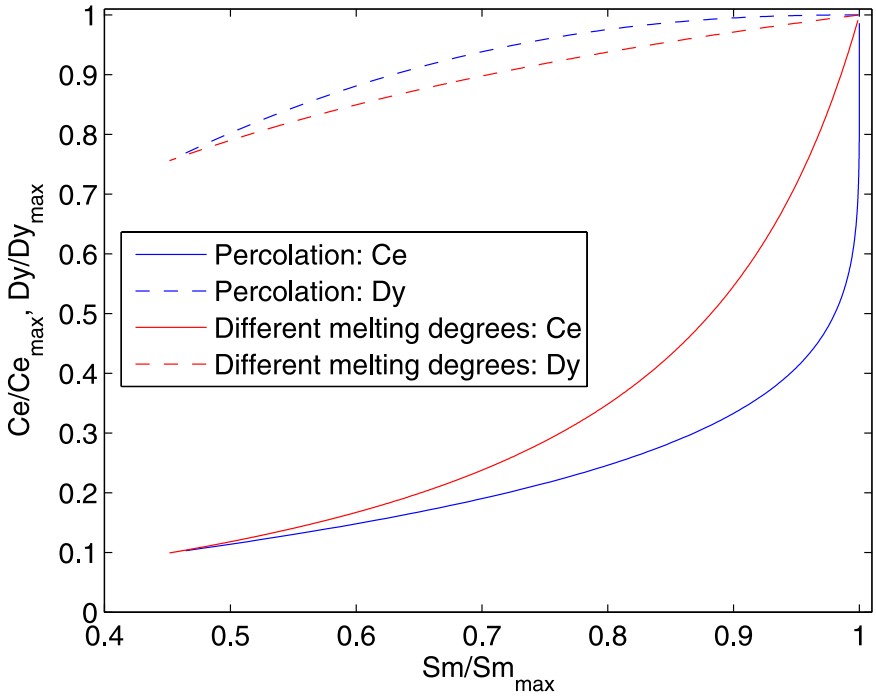

Figure 4. Abundances of Ce, Sm, and Dy predicted by models of percolation and low melting degrees. The abundances of Ce (solid lines) and Dy (dashed lines) are plotted versus Sm abundances. All the abundances are normalized by their maximum values. Blue lines denote predictions of the percolation model, and red lines denote predictions of the low melting degree model.

As one can see from Figure 4, the evolutionary curves for these two cases are similar, and can be hardly distinguished given the uncertainties of observations.

[10] Note that both models (melt percolation and low degrees of melting) assume partial melting at the kimberlite source region, and thus are physically similar. In both cases the melt is assumed to be in equilibrium with the residue, and the maximum possible enrichments are those given by equation (10). However, if the melting degree is low, in order to preserve its unusual composition the melt must segregate within the source region. At higher melt fractions, the melt must leave the depleted source region, and continue to percolate through "fresh" (undepleted) rocks. As discussed in section 5, these different ways of enrichment may result in different eruption sequences.

3. Effects of the Variable Source Composition

[11] At full saturation, the trace element abundances in melt percolating through a solid matrix, or in melt resulting from an infinitesimal melting are inversely proportional to the bulk partition coefficient D (see equation (10)) that depends on the modal composition of the host rocks (equation (6)). According to the mantle xenolith data, the content of the main REE bearing phases, namely garnet and clinopyroxene, may vary widely from 0 to >10% [e.g., *Spetsius and Serenko*, 1990; *Boyd et al.*, 1997; *Schmidberger and Francis*, 2001; *Grégoire et al.*, 2003; *Simon et al.*, 2003] implying a significant variability in the bulk partition coefficient. However, the REE abundances of the saturated melt do not need to be very sensitive to variations in the host rock composition because the dependence of the bulk rock abundances C_0 on x_i may be quite similar to that of the bulk partition coefficient D (equation (10)). In fact, if the modal phases of the host rock are in a diffusive equilibrium, then the reduced REE abundances C_i/D_i should be the same for all mineral phases,

$$\frac{C_{ol}}{D_{ol}} = \frac{C_{opx}}{D_{opx}} = \frac{C_{cpx}}{D_{cpx}} = \frac{C_{gt}}{D_{gt}} = A, \tag{13}$$

where A may depend on parameters affecting the partition coefficients, e.g., the PT conditions under which the equilibration has occurred, and major or

minor element content. Now the whole rock abundance is

$$C_0 = \Sigma_i x_i C_i = A\Sigma_i x_i D_i \propto D, \quad (14)$$

that is, the bulk rock abundances C_0 scale as the bulk partition coefficient D.

[12] In order to compare the model predictions to the data, we use the trace element abundances in ultramafic rocks C_{WM} of *Wedepohl and Muramatsu* [1979], and the partition coefficient D_D calculated for the mantle modal composition proposed by *Dawson* [1980] (assuming $x_{ol} = 0.66$, $x_{opx} = 0.25$, $x_{cpx} = 0.03$, $x_{gt} = 0.06$). It is convenient to express the parameter A (equation (13)) as follows,

$$A = f\frac{C_{WM}}{D_D(T_s)}, \quad (15)$$

where T_s is the source equilibration temperature, and f is a scaling coefficient. As we show below, $D_D(T_s)$ accommodates the principal temperature dependence of the trace element abundances in a saturated melt. The details of the temperature dependence of partition coefficients are described in Appendix B. To the best of our knowledge, there are no data quantifying the pressure dependence of partition coefficients. Therefore the latter is not included in our model. To minimize uncertainties associated with a compositional dependence of partition coefficients, we only consider REE having the same ionic charge, partitioning to the same lattice sites and therefore having a similar dependence on the major and minor element content. Equations (13), (10) and (15) give rise to

$$C_0 = f\frac{C_{WM}}{D_D(T_s)}D(T_s), \quad (16)$$

and

$$y_{sat} = f\frac{C_{WM}}{D_D(T_s)}\frac{D(T_s)}{D(T_k)}. \quad (17)$$

In equations (16) and (17) the coefficient f is an adjustable parameter that accommodates any residual dependence of C_0/D on the modal and chemical composition, and T_k denotes the host temperature during the kimberlitic epoch. Note that the partition coefficients $D(T_s)$ and $D(T_k)$ relate to the same modal and chemical composition, but possibly different temperatures, while $D(T_s)$ and $D_D(T_s)$ relate to the same temperature, but possibly different modal compositions.

[13] The reduced REE abundances in the main REE-bearing phases (clinopyroxene and garnet) are compared in Figure 5 for 13 xenoliths from South Africa [*Grégoire et al.*, 2003; *Simon et al.*, 2003] and 26 xenoliths from Canada [*Schmidberger and Francis*, 2001]. Since the REE abundances in general decrease (with several exceptions like La and Ce), and the partition coefficients increase with the increasing atomic number, the bottom left corner of Figure 5 corresponds to HREE, while the top right corner corresponds to LREE. The line denotes the theoretical prediction (equation (13)). Data shown in Figure 5 reveal a definite correlation between C_{gt}/D_{gt} and C_{cpx}/D_{cpx}, although there exists a substantial scatter especially within the LREE data points. This is not surprising as xenoliths entrained by kimberlites are strongly metasomatized due to interaction with the kimberlitic magmas themselves [e.g., *Harte et al.*, 1993; *Schmidberger and Francis*, 2001; *Simon et al.*, 2003; *Boyd et al.*, 2004; *Burgess and Harte*, 2004]. The metasomatism manifests itself through the grain size heterogeneity [*Simon et al.*, 2003; *Burgess and Harte*, 2004], and large deficiency of the sum of the LREE content in constituent minerals in comparison to the measured bulk rock abundances [*Schmidberger and Francis*, 2001; *Grégoire et al.*, 2003]. In particular, *Schmidberger and Francis* [2001] and *Grégoire et al.* [2003] report that up to 90–99% of La and Ce reside interstitially while the garnet and clinopyroxene contribute to more than 90% of Er, Yb and Lu budget. It follows that HREE in the mantle xenoliths may be considered to be diffusively equilibrated, while LREE are essentially disequilibrated.

[14] This obvious difference in the behavior of the LREE and HREE xenolith abundances can be due to a significant (factor of ~30) decrease in the diffusion coefficients with increasing ionic radii from La to Yb [*van Orman et al.*, 2001]: at temperature 1300°C and pressure 5 GPa the diffusion coefficients of La and Yb are estimated to be $\kappa_{La} = 2 \cdot 10^{-22}$ m^2 s^{-1} and $\kappa_{Yb} = 6 \cdot 10^{-21}$ m^2 s^{-1}, respectively. For a grain size ~1 mm the HREE diffusive equilibration occurs over a timescale of the order of 1 Myr, while the equilibration of LREE takes 10 Myr. If a rock sample was entrained by kimberlites and transported to the surface a few million years after the metasomatism had occurred, it would show partially equilibrated REE distributions, as observed in some xenoliths. On the other hand, a time interval necessary for achieving a full diffusive equilibrium within the grains (10^7 Ma) is likely small compared to the recurrence time of the

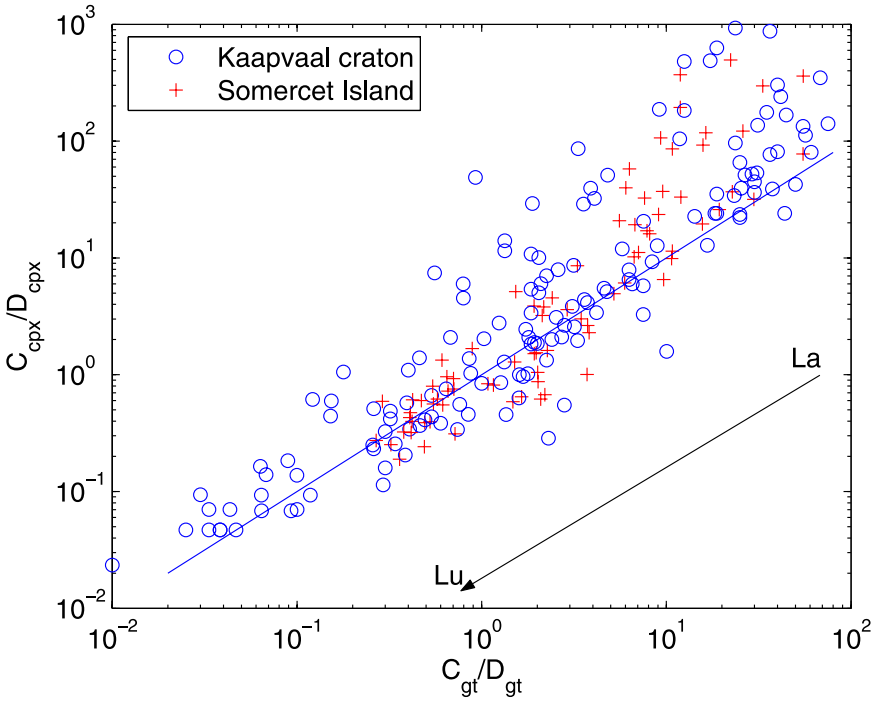

Figure 5. Correlation between the reduced REE abundances C_i/D_i of garnets and clinopyroxenes in xenoliths entrained by South African (circles) [*Grégoire et al.*, 2003; *Simon et al.*, 2003] and Canadian (crosses) [*Schmidberger and Francis*, 2001] kimberlites. The atomic numbers of rare earth elements in general increase from the top right to the bottom left corners of the plot. The line corresponds to the exact equality of the reduced abundances.

major magmatic episodes in the sub-cratonic mantle (e.g., due to mantle plumes). Therefore it is reasonable to assume that the grain size distribution of trace elements among the modal minerals in the kimberlite source region is an equilibrium one, even though the xenoliths do not show the fully equilibrated LREE content. If so, equations (10) and (17) indicate that the saturated melt abundances may only weakly (if at all) depend on the modal composition. This is particularly obvious if $T_s = T_k$, so that the ratio $D(T_s)/D(T_k)$ on the right hand side of equation (17) is exactly unity, and various sources are predicted to generate the same REE patterns even though their whole rock REE abundances may scale as D (and thus be widely different). This behavior is further illustrated in Figures 6 and 7, where the observed whole rock REE abundances in xenoliths from kimberlites from South Africa and Canada are shown along with the reduced ones. For a comparison, the data for every REE species were normalized to the maximum abundance in the xenoliths; similar normalization was applied to the reduced values. The bulk partition coefficients $D(T)$ were calculated using the reported equilibration temperatures and modal compositions [*Grégoire et al.*, 2003; *Simon et al.*, 2003; *Schmidberger and Francis*, 2001].

[15] For disequilibrated LREE the distribution of the reduced values is as wide as, or even wider than the distribution of the bulk rock abundances (see Figure 6). At the same time the distribution of the reduced abundances for equilibrated HREE in Figure 7 is markedly narrower than that of the observed values, even though four samples from the Somerset Island are low-Mg pyroxenites containing as much as 22 to 68% of clinopyroxene compared to 1 to 17% in other samples [*Schmidberger and Francis*, 2001]. This confirms the idea that the saturated HREE abundances of magma percolating through any source sampled by xenoliths are similar even though the source compositions may be very different. As we speculated above, prior to metasomatism the LREE in the kimberlite source rock may partitioned among the modes as close to an equilibrium as HREE. If so, the saturated composition of the melt should not at all depend on the modal composition. This follows from the fact that two rocks with different modal proportions x_i but the same modal abundances C_i can equilibrate with the same melt even though their bulk rock abundances may be substantially different.

[16] If the temperatures T_s and T_k are not the same then the ratio of the partition coefficients

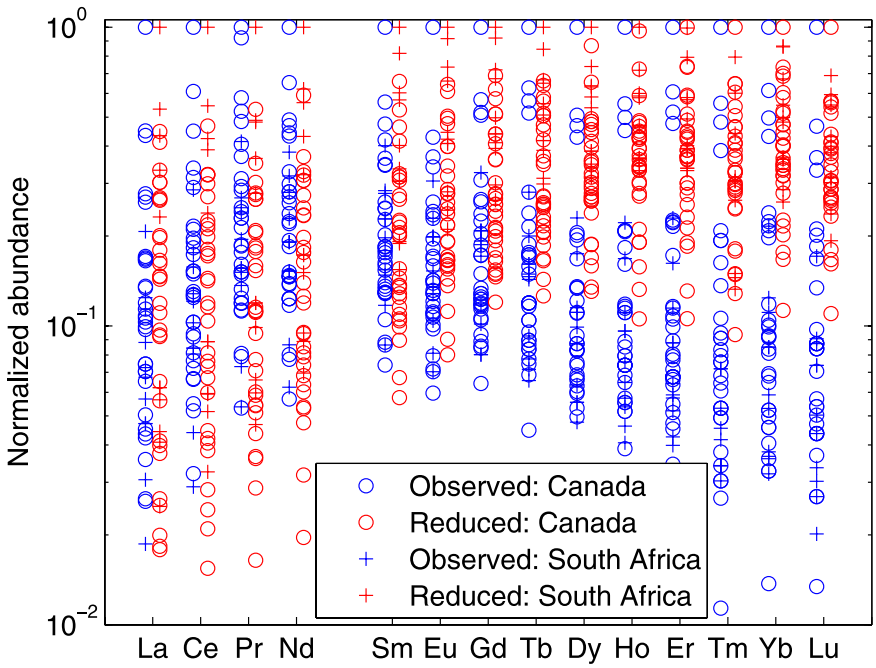

Figure 6. Observed C_0 (blue) and reduced $C_0/D(T)$ (red) REE abundances in xenoliths from the kimberlites of Kaapvaal, South Africa (circles) [*Grégoire et al.*, 2003; *Simon et al.*, 2003], and Somerset Island, Canada (crosses) [*Schmidberger and Francis*, 2001]. For every REE species the measured and reduced data points are normalized to the maximum observed or calculated value, respectively. The respective temperatures and modes are taken from *Schmidberger and Francis* [2001], *Grégoire et al.* [2003], and *Simon et al.* [2003]. The procedure of incorporating the temperature dependence of partition coefficients is described in Appendix B.

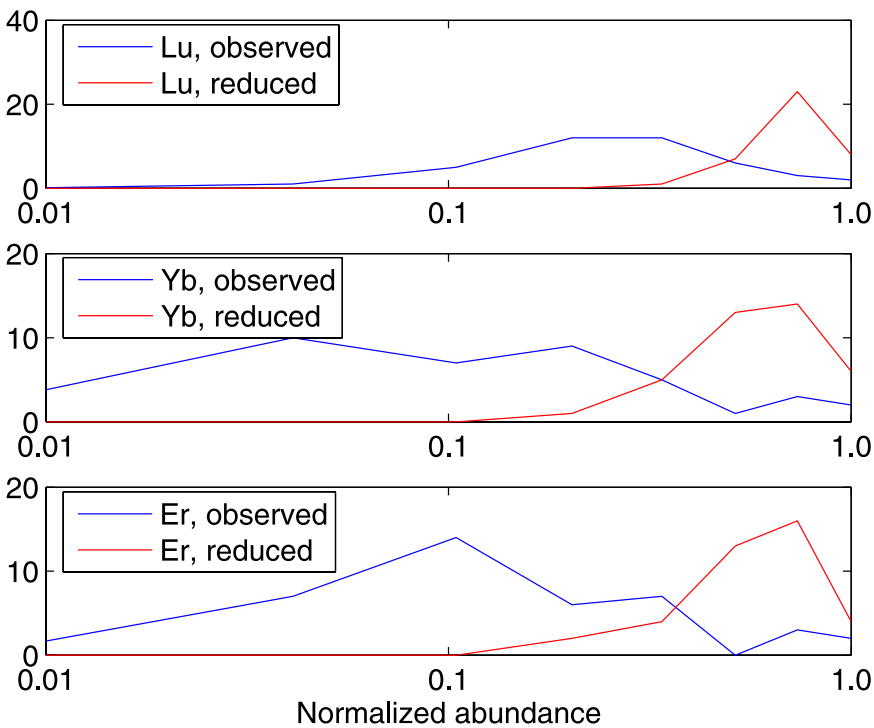

Figure 7. Distribution functions for normalized observed (blue) and reduced (red) abundances of Lu, Yb, and Er in xenoliths from the kimberlites of Kaapvaal, South Africa [*Grégoire et al.*, 2003; *Simon et al.*, 2003], and Somerset Island, Canada [*Schmidberger and Francis*, 2001] (see caption to Figure 6).

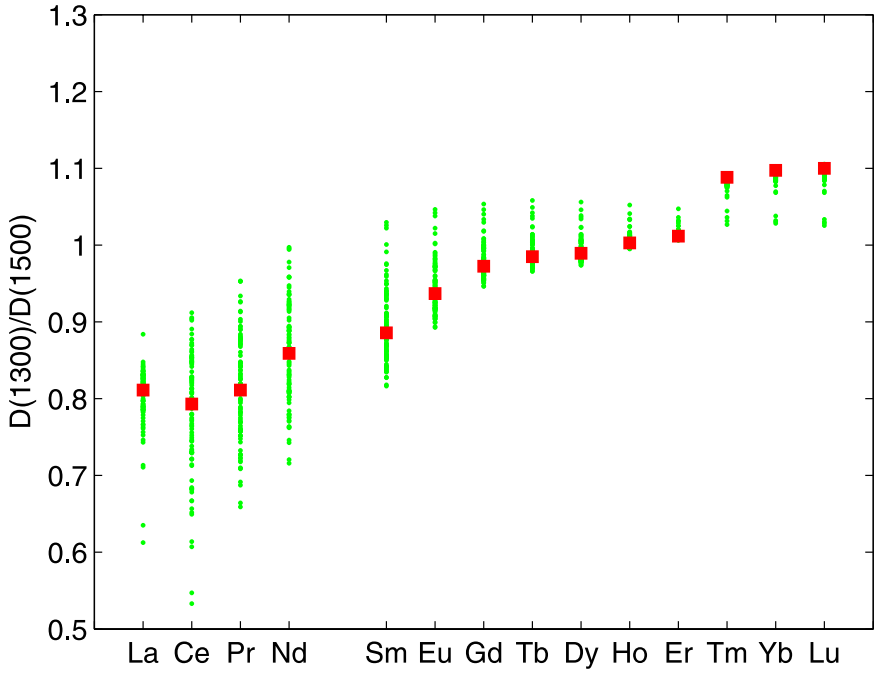

Figure 8. Modal composition dependence of the ratio of bulk diffusion coefficients $D(T_s)/D(T_k)$ for different temperature of source equilibration, T_s, and the "background" temperature during the kimberlite epoch, T_k (see equation (17)). Every green point presents the ratio $D(1300°C)/D(1500°C)$ calculated for modal composition of a real mantle xenolith (the xenolith data are from *Cox et al.* [1973], *Boyd et al.* [1997], *Saltzer et al.* [2001], *Schmidberger and Francis* [2001], *Grégoire et al.* [2003], *Simon et al.* [2003], and *Kopylova and Garo* [2004]). Red squares show the ratio calculated for the mantle modal composition proposed by *Dawson* [1980].

$D(T_s)/D(T_k)$ in equation (17) may introduce some dependence on the modal composition. Figure 8 illustrates this dependence for T_s = 1300°C and T_k = 1500°C. We used modal compositions of 93 xenoliths from South Africa, Yakutia, and Canada compiled from *Cox et al.* [1973]; *Boyd et al.* [1997]; *Saltzer et al.* [2001]; *Grégoire et al.* [2003]; *Simon et al.* [2003]; *Kopylova and Garo* [2004]. The content of clinopyroxene and garnet in these xenoliths range from 0.1 wt% to 14.5 wt%, and from 0.2 wt% to 12.4 wt%, respectively. However, the ratio of the bulk partition coefficients shows relatively small scatter, especially for HREE. Even for cerium which shows the largest variability of the ratio $D(1300)/D(1500)$, 77 out of 93 data points fall into an interval between 0.7 and 0.9, with the other 16 points falling into an interval between 0.5 and 0.7. The red squares in Figure 8 denote the ratio of the bulk partition coefficients calculated assuming the modal composition of *Dawson* [1980]. Taking into account that the latter gives reasonably good agreement with the observations we use the modal composition of *Dawson* [1980] in all numerical estimates below. Accordingly, equation (17) can be simplified to yield

$$y_{sat} = f\frac{C_{WM}}{D_D(T_k)}. \tag{18}$$

[17] We point out that some deviation of the actual REE signatures of kimberlites from those predicted by equation (18) might be expected due to source singularities that are not taken into account by normalizing the source composition to that of *Wedepohl and Muramatsu* [1979]. For example, *Schmidberger and Francis* [2001] report up to a tenfold decrease in the incompatible element contents of clinopyroxene in low-PT (80 to 150 km depth range) xenoliths compared to high PT (estimated depths of 160 to 190 km) xenoliths. The same trend is present in the whole rock LREE abundances in xenoliths from South Africa and Canada [*Grégoire et al.*, 2003; *Schmidberger and Francis*, 2001]. As noted by *Burgess and Harte* [2004], this trend can be due to metasomatic alterations associated with the melt percolation itself. However, similar correlations exist for other

elements; for example, CaO abundance decreases with an increasing depth [*Burgess and Harte*, 2004] along the lherzolite trend proposed by *Sobolev* [1977]. Since REE partition into the Ca ionic sites in both garnet and clinopyroxene [e.g., *Wood and Blundy*, 1997; *Harte and Kirkley*, 1997; *van Westrenen et al.*, 1999], the REE abundances may simply follow the CaO trend, and thus need not manifest a recent metasomatism. We account for this possibility by allowing a range of values of the coefficient f in equation (18). As shown below, the value $f = 1$ gives rise to the predicted REE abundances that are in a good agreement with the maximum observed REE abundances. In order to fit observations, we assume that a decrease in the REE content at the source (represented by factor f) is accompanied by an increase in the source temperature. Specifically, we assume that the value $f = 1$ corresponds to a minimum depth and temperature of the kimberlite source, and values $f < 1$ are representative of greater depths and temperatures. The modeling results presented in the following section assume that values of $f = 1.0$, 0.75, and 0.5 correspond to temperatures in the kimberlite source region of $T_k = 1300°$, 1400°, and 1500°C, respectively.

4. Comparison of Models With Observations

[18] Most existing models of the origin of kimberlites attribute the latter to melting of mantle regions having a peculiar (in fact, kimberlitic) composition. These models may be considered as representing an end member of a spectrum of possible models, with another end member representing a common physicochemical process that operates in a source region of an average mantle composition. The most likely processes for the second class of models are the extremely low degrees of melting, and the chromatographic percolation of melt at finite melt fractions. The two processes predict the same maximum enrichments (see equation (10)), and very similar, though not identical trace element patterns and ratios (see, e.g., Figure 4). In this section we compare predictions of the two process-based models with observations of kimberlites from South Africa [*le Roex et al.*, 2003], Yakutia, Russia [*Golubeva et al.*, 2003] and India [*Chalapathi Rao et al.*, 2004].

[19] As the melt percolates through the solid matrix, the abundances of compatible trace elements (e.g., HREE) reach saturation at the very initial stages of percolation, while saturation in less compatible elements (e.g., LREE) requires more extensive melt migration. Figure 3 illustrates this behavior with evolution of the La and Yb abundances in the first melt batch percolating through unaltered rocks. The difference between LREE and HREE becomes larger still for the subsequent melt batches (also, see equation (A8) of Appendix A). As a consequence, the chondrite normalized [*McDonough and Sun*, 1995] sum of REE, ΣREE_n, resulting from the melt propagation through the source region is predicted to correlate with the characteristic slope of the REE trend $(La/Yb)_n$. Figure 9 compares the REE abundances observed in the South African [*le Roex et al.*, 2003], Yakutian, [*Golubeva et al.*, 2003] and Indian [*Chalapathi Rao et al.*, 2004] kimberlites with those predicted by the two models. Five points from the South African Wesselton Floors sills and Bullfontain pipe shown with filled circles in Figure 9 (samples k5/1, k5/94, K119/2, k8/10 and k8/17 in notation of *le Roex et al.* [2003]) cluster separately in all regression plots for the minor and trace elements. For this reason these five anomalous data points were not included in calculations of the REE envelopes shown in Figure 1. Thin solid lines show how the sum of REE, ΣREE_n and the average slope of a REE pattern, La/Yb evolve as the melt percolates through the matrix. We assume that the percolating melt results from a 3% fusion of a source with chemical and modal compositions proposed by *Wedepohl and Muramatsu* [1979] and *Dawson* [1980], and percolates through a rock with the same initial composition. Dashed lines represent the composition of the melt resulting from melting degrees $0 < \phi < 3\%$. The color of the curves indicates the additional model assumptions (the temperature T_k in the kimberlite source region and values of the respective "depth" factor f): $T_k = 1300°C$, $f = 1.0$ (blue); $T_k = 1400°C$, $f = 0.75$ (green); and $T_k = 1500°C$, $f = 0.5$) (red). Thick lines connect the points of equal fraction of full saturation (magenta: 100%, cyan: 80%, and brown 60%). One can see from Figure 9 that samples from South Africa are highly saturated in REE (saturation in excess of 70%) while the Siberian and Indian kimberlites exhibit lower saturation. Note that because the factor f is the same for all rare earths, any possible variation in f does not affect the La/Yb ratio, resulting in a clockwise rotation of the trajectories with no changes in their length. On the other hand, increases in T_k affect mainly the LREE, thus decreasing both the ΣREE and La/Yb and shortening the trajectories.

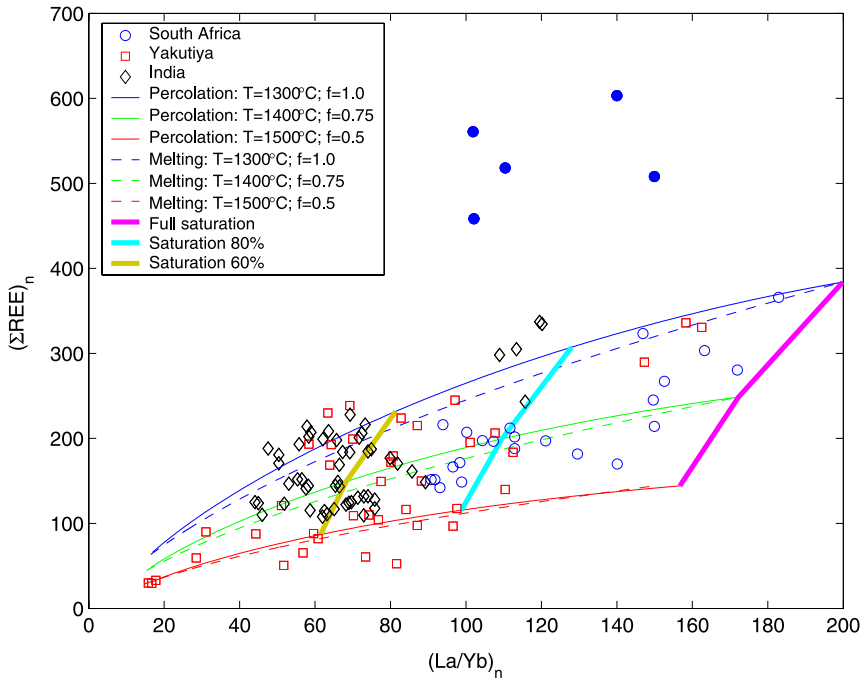

Figure 9. Chondrite normalized [*McDonough and Sun*, 1995] sum of REE, ΣREE_n versus chondrite normalized ratio $(La/Yb)_n$. Data for the South African, Yakutian, and Indian provinces are from *le Roex et al.* [2003], *Golubeva et al.* [2003], and *Chalapathi Rao et al.* [2004], respectively. Five anomalous points from South Africa are shown with filled circles. Thin lines show the model predictions. Solid lines correspond to the percolation model (equation (8)) with C_0/D given by equation (18), and dashed lines represent the composition of melt resulting from different degrees of melting (equation (12)). The line color denotes the temperature in the kimberlite source region and the value of f: $T_k = 1300°C$, $f = 1$ (blue); $T_k = 1400°C$, $f = 0.75$ (green); $T_k = 1500°C$, $f = 0.5$ (red). Thick lines connect the points of equal fraction of full saturation (magenta: 100%, cyan: 80%, and brown 60%).

[20] The predicted trace element content in a propagating batch of melt follows trajectories seen in Figure 9 from left to right, i.e., increasing the La/Yb ratio, and the total REE content, and eventually evolving from essentially undersaturated values characteristic of 3% melting to a composition corresponding to an infinitesimal melt fraction. These results may reconcile the relatively large melt fractions (>1%) that might be necessary for the melt segregation [*Faul*, 1997; *Wark and Watson*, 1998; *Liang et al.*, 2001] with high REE enrichments observed in kimberlites. The dashed lines in Figure 9 represent the melt composition resulting from different degrees of melting. Note that the melt fraction increases from $\phi = 0$ in the top right corner in Figure 9 to $\phi = 3\%$ in the bottom left corner. Figures 10 and 11 display the REE abundances in South African [*le Roex et al.*, 2003] and Indian [*Chalapathi Rao et al.*, 2004] kimberlites as a function of the samarium abundance [*Navon and Stolper*, 1987]. All abundances are normalized by the maximum observed ones. Thin lines represent the evolutionary curves calculated using the percolation model for a melt resulting from a $\phi_0 = 3\%$ melting, and percolating through the matrix of the same composition. Thick lines connect points corresponding to the full saturation of the theoretical composition with the corresponding chemical elements. Every line denotes a certain chemical element as indicated by the line color, while the black line indicates equal normalized abundances of an REE element and samarium. The calculated abundances were normalized to the saturated ones predicted by the model for $T_k = 1300°C$, $f = 1$. Note that because the composition of the source rock and of the rocks through which melts eventually percolate is assumed to be the same, the calculated normalized abundances turn out to be independent of the source ones. As one can see from Figure 10, the South African data points lie along the line of equal normalized abundances and thick lines indicating that the South African kimberlites are close to the full saturation with REE, and that the observed REE abundances are highly correlated. The data correlation is especially good for the LREE (Figure 10a). MREE and HREE show some scatter which increases from LREE to HREE. From the viewpoint of the percolation model such a scatter is

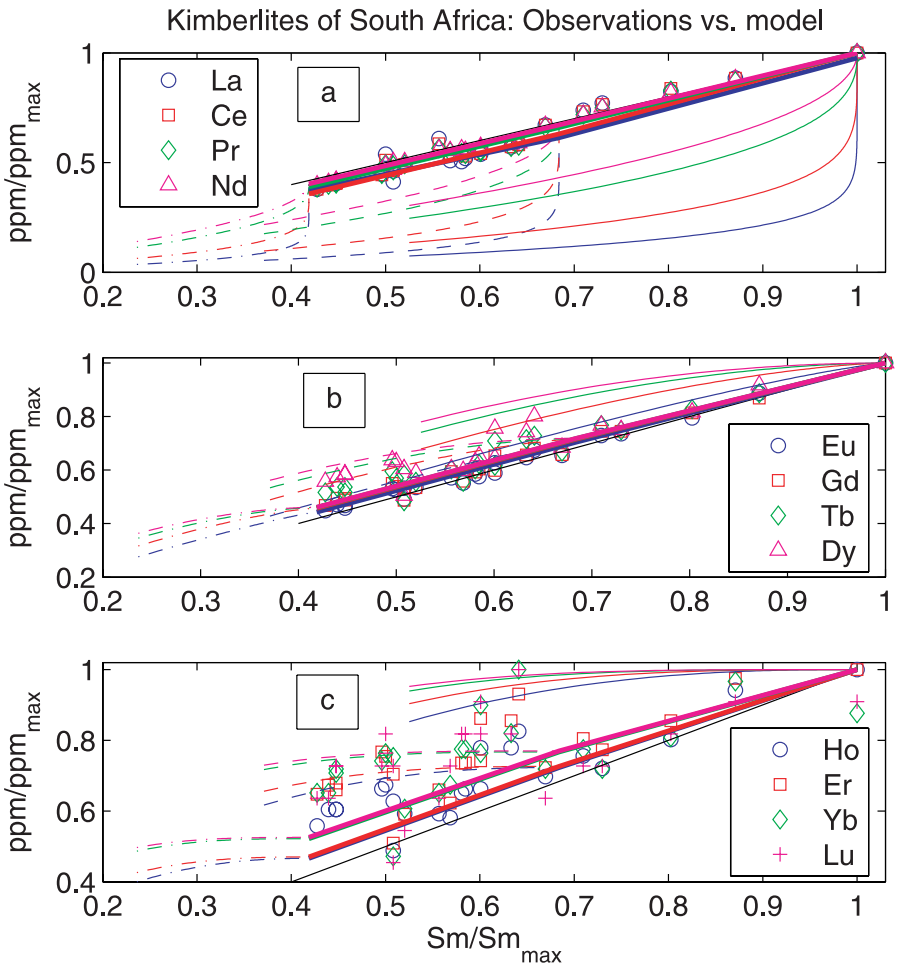

Figure 10. Abundances of the REE elements in kimberlites from South Africa [*le Roex et al.*, 2003] are shown against the samarium abundance. All abundances are normalized by the maximum values (the five points marked by filled circles in Figure 9 are not included). Thin lines show predictions of the percolation model for different values of the model parameters: T_k = 1300°C, f = 1 (solid lines); T_k = 1400°C, f = 0.75 (dashed lines); T_k = 1500°C, f = 0.75 (dash-dotted lines). Every line denotes a certain chemical element as indicated by the line color (blue, red, green, or magenta) and shown in the legend. Thick lines connect points corresponding to the full saturation of the theoretical composition with the corresponding chemical elements. The black line indicates equal normalized abundances of an REE element and samarium. So, the area below the black line corresponds to elements that are less compatible than samarium, while the area above the line of equal abundances corresponds to more compatible elements. (a) La, Ce, Pr, Nd; (b) Eu, Gd, Tb, Dy; (c) Ho, Er, Yb, Lu.

expected, because in order to saturate in incompatible LREE, melt must percolate over a much larger distance compared to that necessary for a melt saturation with HREE. Therefore the LREE abundances likely reflect the mantle composition averaged over a larger region compared to that represented the HREE abundances. As a consequence the HREE abundances are expected to show more variability than the LREE and MREE abundances, as actually observed. We point out that the low degree melting model does not predict any systematic dependence of the data scatter on a species compatibility.

[21] Data shown in Figure 10 suggest that LREE are very close to a full saturation. Moreover the normalized abundances of different elements are practically coincident. This implies that at least for LREE the factor f does not depend on the atomic number of a species. The last conclusion stems from the following considerations. Let us assume that f in fact depends on the atomic number and temperature $f = f_{el}(T_k)$ (where el = La, Ce, ...) so that for the reference temperature 1300°C the values of f are the same for all REE,

$$f_{el}(1300) = 1, \tag{19}$$

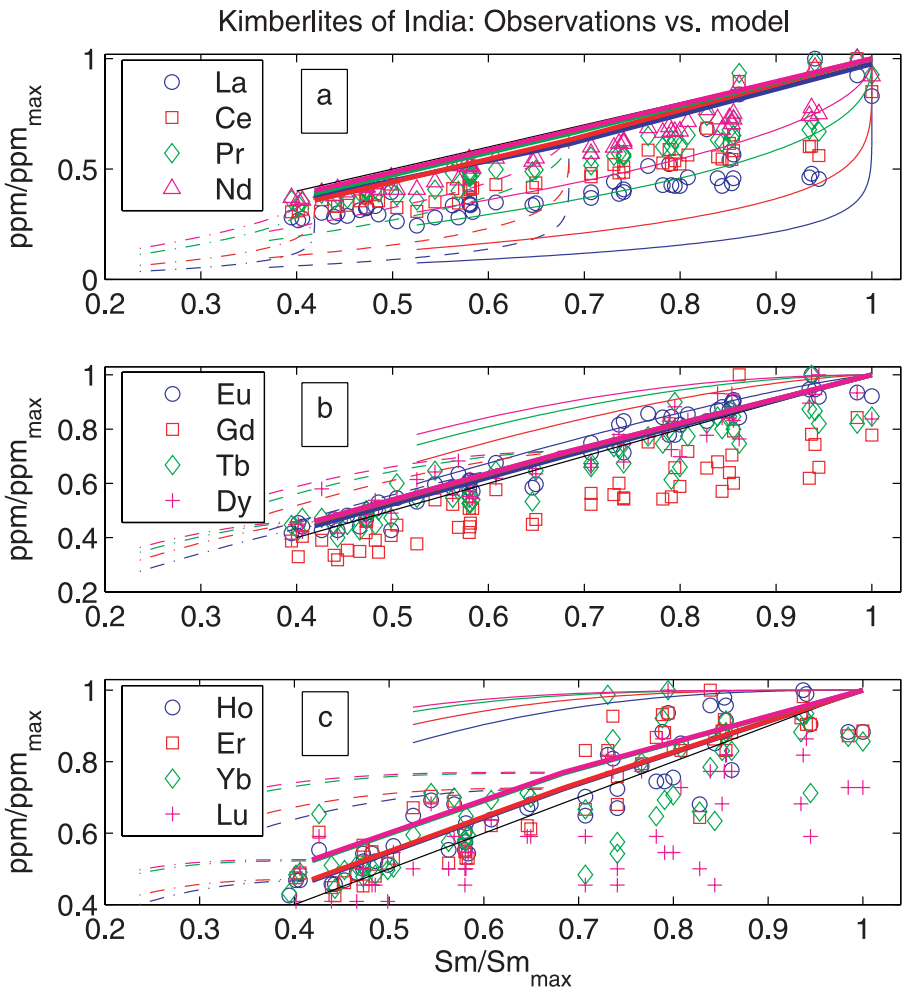

Figure 11. Abundances of the REE elements in kimberlites from India *Chalapathi Rao et al.* [2004]. Notation is the same as in Figure 10.

as discussed above, but the factors f might be different at higher temperatures. Then, for instance, for La and Sm the saturated abundances predicted by equation (18) can be written as

$$y_{satLa}(T_k) = f_{La}(T_k)\frac{C_{LaWM}}{D_{La}(T_k)}, \tag{20}$$

$$y_{satSm}(T_k) = f_{Sm}(T_k)\frac{C_{SmWM}}{D_{Sm}(T_k)}. \tag{21}$$

After normalization of these abundances by their maximum values at T_k = 1300°C one finds

$$Y_{La}(T_k) = \frac{D_{La}(1300)}{D_{La}(T_k)}\frac{f_{La}(T_k)}{f_{La}(1300)}, \tag{22}$$

$$Y_{Sm}(T_k) = \frac{D_{Sm}(1300)}{D_{Sm}(T_k)}\frac{f_{Sm}(T_k)}{f_{Sm}(1300)}, \tag{23}$$

where $Y_{La}(T_k)$ and $Y_{Sm}(T_k)$ denote the normalized saturated abundances,

$$Y_{La}(T_k) = \frac{y_{satLa}(T_k)}{y_{satLa}(1300)}; Y_{Sm}(T_k) = \frac{y_{satSm}(T_k)}{y_{satSm}(1300)}. \tag{24}$$

For LREE in kimberlites from South Africa,

$$Y_{La}(T_k) = Y_{Sm}(T_k). \tag{25}$$

The ratios of partition coefficients at different (but fixed) temperatures are almost the same for La and Sm, and for all LREE (e.g., $D_{La}(1300)/D_{La}(1500) = 0.784$ while $D_{Sm}(1300)/D_{Sm}(1500) = 0.833$; see Appendix B). Neglecting this difference and taking into account equation (19), from equations (22) to (25) one obtains

$$f_{La}(T_k) = f_{Sm}(T_k). \tag{26}$$

Results shown in Figure 10 present a very stringent test of the constancy of f. Let us assume that at

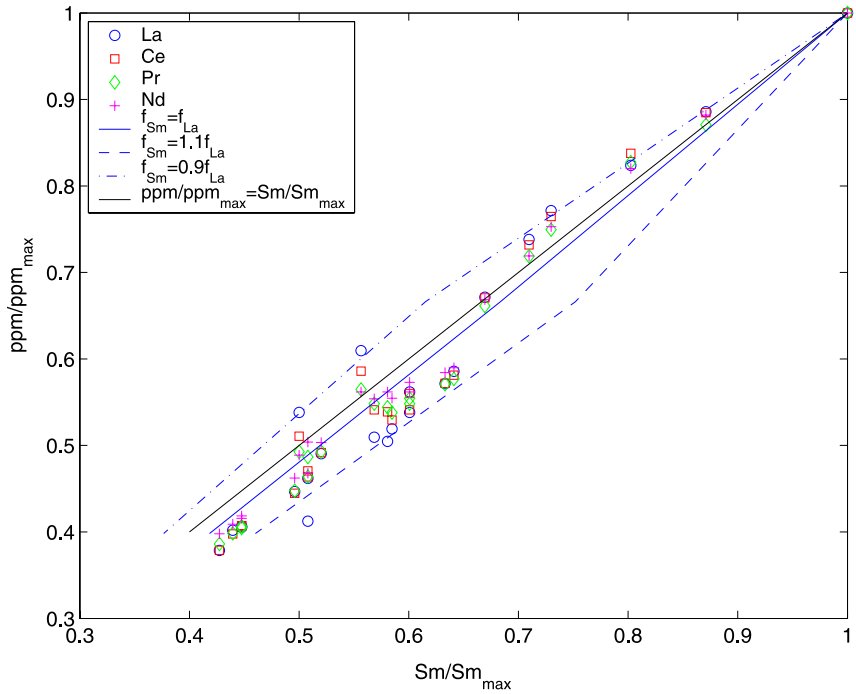

Figure 12. Independence of the factor *f* of the REE atomic number: comparison with the LREE observations in the South African kimberlites. As in Figure 10a the normalized abundances of La, Ce, Pr, and Nd are plotted against the normalized abundance of Sm with the black line corresponding to the equal values of the normalized abundances. Blue lines show the saturated abundances of the lanthanum. The solid line represents calculations assuming the same values of the factor *f* for both La and Sm; the dashed lines represent calculations assuming $f = 1$ for both La and Sm at temperature of 1300°C and differing by ±10% at elevated temperatures (1400 and 1500°C).

elevated temperatures (e.g., 1400°C and 1500°C) factors *f* for Sm differ from those for La and Dy by as little as ±10%. The resulting plots $Y_{La}(T_k)$ and $Y_{Dy}(T_k)$ vs. $Y_{Sm}(T_k)$ are shown in Figures 12 and 13 along with the LREE and MREE data from the South African kimberlites [*le Roex et al.*, 2003]. One can see that nearly all data points in Figure 12, and the majority of data points in Figure 13 reside within the ±10% bounds, so that the factor *f* is essentially independent of atomic number for both LREE and MREE. It seems reasonable to assume that the same holds for all REE. The deduced constancy of the parameter *f* in data from the South African kimberlites means that the abundances of different REE are not independent. The data indicate that the contents of individual trace elements are highly correlated, a phenomenon that will be hereafter referred to as the coherency of REE patterns. This phenomenon is in a full agreement with the apparent parallelism of the REE patterns which have too few intersections to be random. The inferred coherency most likely results from some process or a mechanism that equally affects the abundances of all REE. Since all REE partition into Ca sites in the lattice of both garnet and clinopyroxene [e.g., *Wood and Blundy*, 1997; *Harte and Kirkley*, 1997; *van Westrenen et al.*, 1999], one may speculate that the coherent variations of the REE abundances may simply result from variations in the number of lattice sites available for REE, i.e., from variations in Ca content in the source rock. Recall that in order to fit the model to the observed ΣREE and La/Yb values (see Figure 9) we had to assume that a decrease in the overall REE contents in the source rock (modeled by decreases in the effective saturation parameter *f*) is accompanied by an increase in the source temperature. The assumed variations in temperature and saturation may be naturally explained in terms of increases in the source depth, as it is well established that the Ca content decreases with depth along the so-called "lherzolite trend" [*Sobolev*, 1977; *Burgess and Harte*, 2004].

[22] The Indian kimberlites show much more diversity in the REE compared to the African kimberlites. Although the data points in Figures 11a–11c cluster along the lines of maximum abundances similarly to the South Africa data, the data point clouds in Figure 11 are much wider than those in Figure 10. Note, however, that LREE in the Indian kimberlites (Figure 11a) show a clear

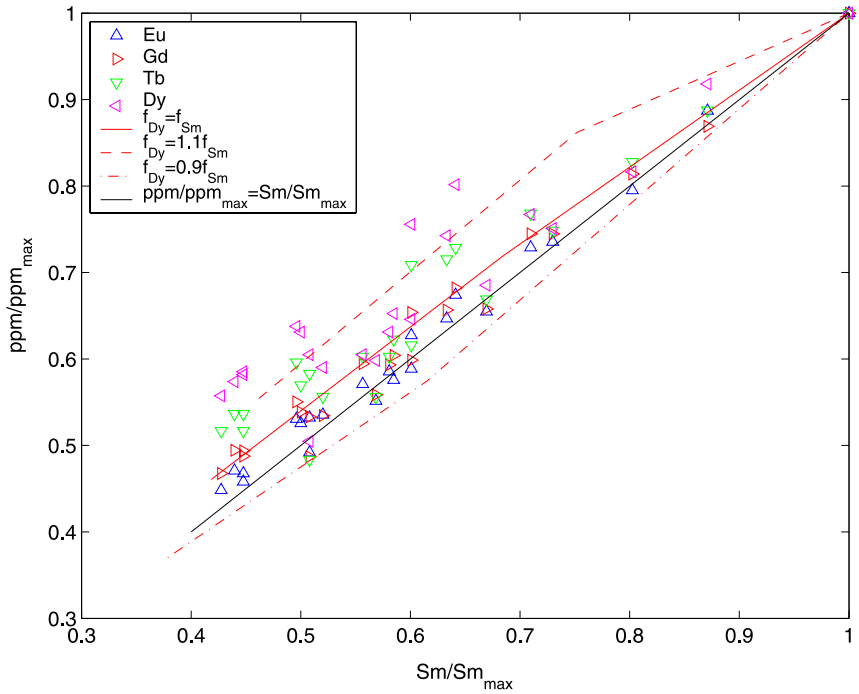

Figure 13. Independence of the factor f of the REE atomic number: comparison with the MREE observations in the South African kimberlites. The normalized abundances of Eu, Gd, Tb, and Dy are plotted against the normalized abundance of Sm. Red lines show the saturated abundances of dysprosium. The solid line represents calculations assuming the same values of the factor f for both Dy and Sm; the dashed lines represent calculations assuming $f = 1$ for both Dy and Sm at temperature of 1300°C and differing by ±10% at elevated temperatures (1400 and 1500°C). Other notation is the same as in Figure 12.

ordering (bottom-up: La, Ce, Pr, Nd) that is in agreement with their relative incompatibility. This lends support to the percolation and low melting degree models that predict such a trend. The order of species in Figures 11b and 11c does not match their compatibility. This is especially evident for Dy and Lu, although these elements show some irregularity in the REE patterns (e.g., Figure 1), which might at least partially account for the observed disordering.

[23] The REE patterns predicted by the percolation and low melting degree models are shown in Figure 14. The envelopes of the REE patterns from the South African, Yakutian, and Indian kimberlites are the same as those in Figure 1. The theoretical patterns correspond to T_k = 1300°C, f = 1.0 (blue), T_k = 1400°C f = 0.75 (green), T_k = 1500°C, f = 0.5 (red). Thick lines refer to the saturated patterns and coincide with those resulting from the infinitesimal degree of melting. Thin blue lines show unsaturated patterns arising from melt percolation at the source temperature T_k = 1300° and f = 1.0. The saturation (100%, 66%, 40%, and 15%) is indicated by the curves as a La abundance with respect to the saturated value. Note that a sequence of patterns relating to the same source conditions form a characteristic fan-like structure noted by *le Roex et al.* [2003] in the South African data. The unsaturated patterns for different source conditions form the same fan like structures shifted to lower values. The unsaturated patterns arising from a sequence of melting degrees (not shown) are almost indistinguishable from the patterns predicted by the percolation model given the percentage of La saturation. The melting degrees necessary to produce melts that are enriched with La at the level of 66%, 40%, and 15% of the infinitesimal melt are 0.13%, 0.35%, and 1.3%, respectively. The melt saturation of 70% requires a melt fraction of 0.1%, and the melt saturations greater than 90% require melt fractions lower than 0.02%. As pointed out in the Introduction, such low degrees of melting may result in extremely low permeabilities that might preclude the efficient melt segregation.

5. Discussion

[24] Analysis of the trace element chemistry of kimberlites reveals a remarkable similarity of the

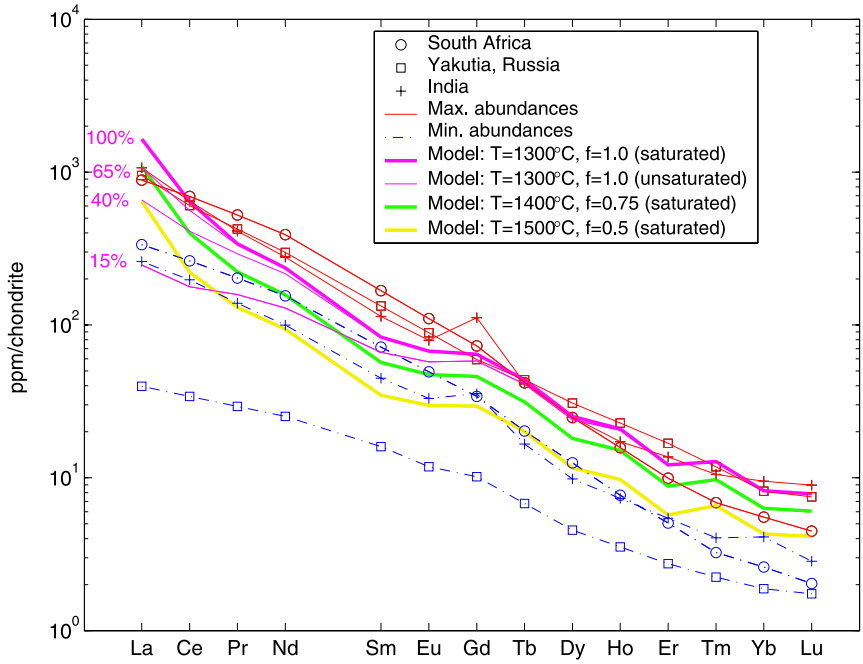

Figure 14. Comparison of the observed and modeled REE patterns. The envelopes of the REE patterns from the South African, Yakutian, and Indian kimberlites are the same as in Figure 1. The theoretical patterns are calculated for different values of f and T_k: $T_k = 1300°C$, $f = 1.0$ (magenta lines), $T_k = 1400°C$ $f = 0.75$ (green line), $T_k = 1500°C$, $f = 0.5$ (yellow line). Thick lines denote the saturated patterns and coincide with those resulting from the infinitesimal melting. Thin blue lines show unsaturated patterns arising from melt percolation at the source temperature $T_k = 1300°$ and $f = 1.0$. The indicated saturations (100%, 66%, 40%, and 15%) represent a ratio of the La abundance to its saturated value.

REE patterns of kimberlitic magmas from different provinces worldwide (Figure 1). Moreover, the REE patterns from some provinces (e.g., South Africa) exhibit a high correlation between individual trace elements, at least for LREE and MREE (Figure 10). We suggest that the unusual chemical signatures of kimberlites are best explained in terms of a common physical process that operates in an ordinary source region in the subcratonic mantle. The two most likely candidates for such a process are the melt percolation through the host rocks [*Navon and Stolper*, 1987; *Harte et al.*, 1993; *McKenzie*, 1989; *Burgess and Harte*, 2004], and the low degree melting [*Dawson*, 1971; *Eggler and Wendlandt*, 1979; *Wyllie*, 1980; *Eggler*, 1989]. These processes share many similarities. Both processes imply partial melting of the host rocks, segregation of melt due to a porous flow, and predict the same maximum melt enrichments and similar undersaturated patterns of trace elements.

[25] If the source rocks are chemically equilibrated, the REE abundances predicted by both processes only weakly, if at all, depend on the modal composition of the source rocks. This independence of the modal composition means that for a given trace element abundance in the modal minerals, the rock equilibrates with the same saturated melt independently of its mode proportions. This may explain the nearly coincident values of the maximum REE abundances in different kimberlite provinces. On the other hand, we demonstrated that the observed REE abundances may be explained in terms of a relatively limited (only a factor of two) variations in the saturation parameter f in equations (17) and (18). We speculate that this is the range of variability in saturation of the modal minerals with REE. Note that the bulk rock abundances may show much larger variations due to the variability in the modal composition. Moreover, the coherency of the REE patterns observed in kimberlites from South Africa [*le Roex et al.*, 2003] (Figure 10) suggests that the REE abundances may be controlled by a single phenomenon that uniformly affects abundances of all trace elements. Since all rare earths partition into the ionic sites of Ca in the lattice of garnet and clinopyroxene, we hypothesize that the controlling phenomenon is the calcium content in the source rocks. We find that the observed REE abundances in kimberlites are best explained if we assume that the overall enrichment of the source region in REE decreases with the

increasing temperature. In our models, such a decrease is simulated by varying the effective saturation parameter *f*. Since the source temperature is expected to increase with depth, the assumed variations in parameter *f* may be interpreted in terms of a decrease in the Ca content along the lherzolite trend [*Sobolev*, 1977; *Burgess and Harte*, 2004]. Therefore one can speculate that the depth dependence of the Ca content may explain the observed variations in the REE abundances in kimberlites from South Africa provided that the latter were derived from sources of various depths.

[26] The principal difference between the percolation model and the low melting degree model is twofold. First, the percolation model allows for relatively large (e.g., ~1–3%) melt fractions in the source region, and thus the efficient melt extraction. Second, in order to preserve their unusual composition the products of the low degree melting must segregate in situ, while the chromatographic enrichment requires that the melt percolates beyond the source region. Percolation is widely believed to be the initial (or perhaps even dominant) mechanism of melt segregation [e.g., *Aharonov et al.*, 1995; *Connolly and Podladchikov*, 1998; *Spiegelman and Kelemen*, 2003]. Melt percolation is associated with metasomatic alterations due to a robust diffusive exchange between the melt and solid matrix, as well as due to reactions of dissolution and precipitation [*Harte et al.*, 1993]. The fingerprints of the metasomatism of this type are commonly observed in the deep mantle xenoliths [e.g., *Erlank et al.*, 1987; *Menzies et al.*, 1987; *Smith and Boyd*, 1987; *Harte*, 1987; *Harte et al.*, 1993; *Grégoire et al.*, 2003; *Ionov et al.*, 2002b; *le Roex et al.*, 2003; *Burgess and Harte*, 2004]. Note that the grain rim enrichment typically seen in the metasomatized xenoliths is a direct evidence of melt percolation outside of the melting region, since melting under conditions of diffusive equilibrium results in depletion, rather than enrichment of the grain rims. Therefore the metasomatized xenoliths lend support to the basic assumption of the chromatographic model, namely that the kimberlitic melts percolated over large distances upon leaving their source regions.

[27] As the HREE abundances reach saturation at the initial stages of percolation, much more rapidly compared to the LREE abundances, the REE patterns of undersaturated magmas have the average slope, $(La/Yb)_n$, that is smaller than the slope corresponding to the saturated magmas. The predicted REE patterns of magmas of different saturation have a characteristic diverging fan-like structure that has been indeed identified in the data [*le Roex et al.*, 2003]. The non-random character of the REE patterns, together with the inferred correlation between the REE abundances in the South African (Figure 10), and to a lesser extent Indian (Figure 11) kimberlites lend further support to a model of the kimberlite origin implying a single stage process operating in an ordinary source. Note that the alternative theories that appeal to multiple processes of melting and metasomatism cannot readily explain close resemblance of the trace element patterns in kimberlites generated in different locations and at different times.

[28] We point out that the data shown in Figures 1, 9, 10, 11, and 14 might be also explained in terms of various degrees of melting in the source region. While the two models cannot be distinguished on the basis of the geochemical data alone, differences in the melting degrees assumed by the two models may be in principle distinguished using geologic observations. It is well established that the transport of kimberlites through the sub-solidus lithosphere occurs in dikes [*Spence and Turcotte*, 1990; *Lister and Kerr*, 1991]. Such trans-lithospheric dikes must drain sizeable volumes of segregated melt [*Rubin*, 1998]. The model assuming variable degrees of melting implies that segregation of a given volume of melt necessary to fill a dike at a low melt fraction involves a larger volume of the source rock, and occurs slower, than segregation at a higher melt fraction. At a lower melt fraction, magma needs to percolate a larger distance through a less permeable matrix, so that the segregation time scales as ϕ^{-2} to ϕ^{-3}, depending on how the permeability scales with the melt fraction. For example, the segregation of magma at a melt fraction of the order of ~0.1% would take 10^2 to 10^3 longer than the segregation of magma at a 1% melt fraction. This implies that the least enriched (high melt fraction) magmas would be expected to erupt first, and the most enriched magmas would be expected to erupt last.

[29] The associated time lag between eruptions of the least and most enriched magmas may be observable. In order to segregate, melts have to percolate over distances exceeding a characteristic spacing between individual kimberlite vents of the order of hundreds of meters to kilometers [*Mitchell*, 1986]. Assuming the corresponding percolation distance of the order of 1 to 10 km, the melting degree of the order of ~0.1%, the driving pressure gradient of the order of 1% of ρg, where ρ is the rock

density and g is the acceleration due to gravity, the grain size of 1 to 3 mm, and the laboratory-derived relationship between porosity and permeability [*Wark and Watson*, 1998; *Liang et al.*, 2001], the estimated velocity of melt segregation is of the order of 0.3 to 3 mm/yr, and the segregation timescale is of the order of 0.3 to 30 Ma. We note that the characteristic duration of magmatic activity in individual kimberlite fields is of the order of 10 Ma [e.g., *Vladimirov et al.*, 1990; *Heaman et al.*, 2003a]. Given that melts resulting from higher degrees of melting are expected to segregate on much smaller timescales, the corresponding time lag should be of the order of the timescale for segregation of the most enriched melt, perhaps large enough to be detectable by geochronologic techniques. The percolation-saturation model, on the other hand, does not predict any correlation between the melt fraction and the degree of melt saturation with trace elements, implying no significant time delay between eruptions of less and more enriched magmas. In fact, an eruption sequence predicted by the chromatographic model is opposite to a sequence associated with different degrees of melting, as the most enriched melts are expected to emerge on top of a melting column [e.g., *Navon and Stolper*, 1987].

[30] Overall, our results demonstrate that the geochemical peculiarities and variability in the source composition likely play a much smaller role in the generation of kimberlites than usually assumed. The kimberlites may indeed originate from a mantle of an ordinary composition provided certain conditions, such as melting at large depth, and extended melt percolation beyond the source region, are met. Such conditions may be typical for thermal activation of a subcratonic mantle (e.g., due to mantle plumes), and explain the similar chemical composition of kimberlites from different provinces around the world.

6. Conclusions

[31] Our analysis of geochemical data on kimberlites from South Africa, India, and Yakutia (Russia) indicates that differences in the REE abundances between different provinces are smaller than the REE variability within any single province. The maximum REE abundances are practically identical in the three kimberlite provinces. The REE patterns of African kimberlites are also extremely coherent (that is, the REE abundances are highly correlated, at least for the light and middle REE). We argue that these similarities are due to a common process operating in the kimberlite source region. The low degree melting and diffusive exchange and metasomatic reactions in the result of extensive percolation of melt are the most likely candidates for such a process. Our preferred model is the extensive melt percolation, as it avoids a problem of melt extraction from a low permeability matrix, and is supported by the xenolith data. We point out that the two models (low degree melting, and percolation) predict different eruption sequences of magmas with different degrees of enrichment, potentially allowing the model discrimination using accurate dating of the erupted samples. The trace element signatures of melt that experienced multiple chemical interactions with the host rocks are universal in that they are independent of the degree of melting, and the modal composition of the source. This suggests that the effect of the source composition on the observed geochemical signatures of kimberlites may be much less than usually assumed, and, in fact, kimberlites may have been derived from a mantle source of an ordinary composition. The REE patterns predicted by the percolation model are in a good agreement with those observed in kimberlites from South Africa, Yakutia, and India. The undersaturated REE patterns form characteristic diverging fan-like structures that result from a much more rapid saturation of melt with heavy REE compared to light REE. Such patterns are indeed observed in data from the South African kimberlites. The inferred coherency of the REE patterns in the South African kimberlites implies a common mechanism (or a combination of mechanisms) that affects the abundances of all REE in kimberlites. We propose that the corresponding controlling mechanism is the calcium abundance in the source rocks, as the Ca content determines the total number of lattice sites available for REE. In this case, a decrease in the overall enrichment of the source rock with depth assumed in our model can be naturally interpreted in terms of a decrease in Ca content along the well-known lherzolite trend.

Appendix A: Solution to Recurrent Equations

[32] Equations (4) and (5) from section 2 can be written as

$$y_{1s} = q y_{1s-1} + \frac{C_0}{\phi + D}, \tag{A1}$$

$$y_{ns} = q y_{ns-1} + \frac{C_{ns}}{\phi + D}, n > 1. \tag{A2}$$

Table B1. Partition Coefficients Mineral/Melt

REE	Ol/Melt	Opx/Melt	Cpx/Melt	Gt/Melt
La	0.0001	0.0002	0.054	0.0016
Ce	0.0002	0.0004	0.086	0.008
Pr	0.0003	0.0006	0.139	0.04
Nd	0.0004	0.001	0.187	0.06
Sm	0.00044	0.003	0.291	0.239
Eu	0.00056	0.004	0.35	0.378
Gd	0.001	0.0128	0.4	0.6
Tb	0.00104	0.0186	0.429	0.85
Dy	0.0014	0.0261	0.442	1.072
Ho	0.00184	0.0356	0.439	1.8
Er	0.00236	0.0474	0.436	2.802
Tm	0.00296	0.0617	0.433	3.5
Yb	0.00364	0.0787	0.43	5
Lu	0.0044	0.0986	0.427	6

where $q = \phi/(\phi + D)$ is the quotient of the geometric series.

[33] We assume that every batch of melt entering the chromatographic column has the same element abundance y_0 (i.e., $y_{n0} = y_0$). The bulk element abundance in a fresh matrix is assumed to be constant and equals C_0. The n-th batch of melt interacts with a solid that has the element abundance corresponding to chemical equilibration with the preceding melt batch. Thus $C_{1s} = C_0$, and $C_{ns} = Dy_{n-1s} (n > 1)$.

[34] Introducing a new parameter $Q = D/(\phi + D)$, one can rewrite equations (A1) and (A2),

$$y_{1s} = qy_{1s-1} + \frac{Q}{D}C_0, \tag{A3}$$

$$y_{ns} = qy_{ns-1} + Qy_{n-1s}, n > 1. \tag{A4}$$

Note that the first terms on the right hand side of equations (A3) and (A4) contribute the terms $q^s y_0$, while the second terms give rise to a geometric progression-like series,

$$y_{1s} = q^s y_0 + Q\frac{C_0}{D}\Sigma_{k=0}^{s-1}q^k = \frac{C_0}{D} + q^s\left(y_0 - \frac{C_0}{D}\right), \tag{A5}$$

$$y_{ns} = q^s y_0 + Q\Sigma_{k=0}^{s-1}q^k y_{n-1s-k}, n > 1. \tag{A6}$$

Substituting equation (A5) to the right hand side of equation (A6), and evaluating the latter for $n = 2$, $n = 3$, and so forth, one can obtain a general solution as follows,

$$y_{ns} = \frac{C_0}{D} + q^s\left(y_0 - \frac{C_0}{D}\right)B(n,s), \tag{A7}$$

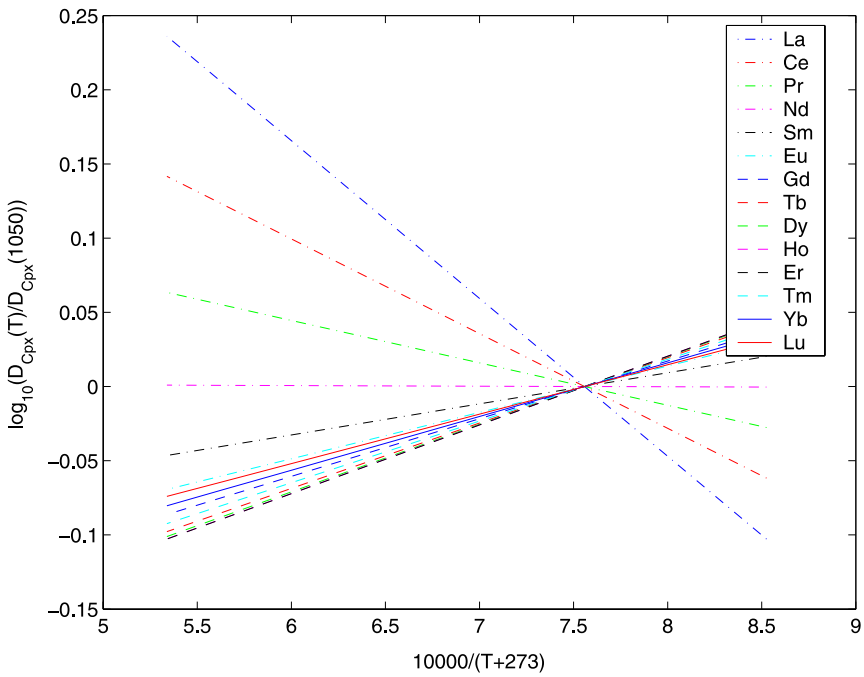

Figure B1. REE partition coefficients cpx/melt normalized by their values at the reference temperature 1050°C.

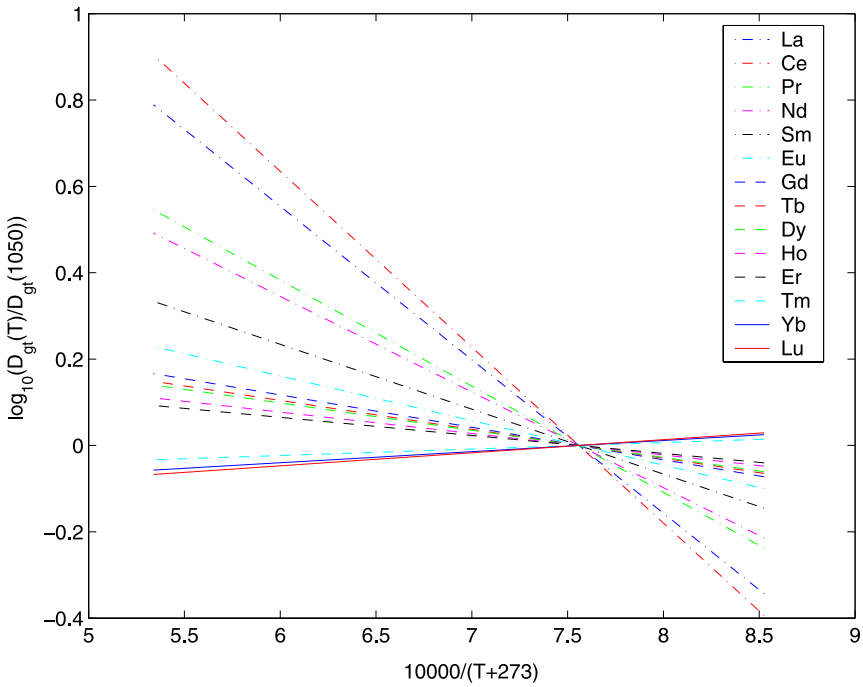

Figure B2. REE partition coefficients gt/melt normalized by their values at the reference temperature 1050°C.

where B_{ns} are recurrent numeric coefficients

$$B(n,s) = 1 + Q\Sigma_{k=1}^{s} B(n-1,k); B(1,s) = 1. \qquad \text{(A8)}$$

Appendix B: Partition Coefficients

[35] The values of partition coefficients used in this paper were compiled from several studies [*Ionov et al.*, 2002a; *le Roex et al.*, 2003; *Burgess and Harte*, 2004]. Obviously, the choice is non-unique. Moreover, the published values do not correspond to either specific values of temperature and pressure, or a particular chemical composition. To avoid using an inconsistent set of partition coefficients, we applied some smoothening to the data for garnet to ensure a trend noted by *Onuma et al.* [1968]. This smoothening had little effect on the calculated REE patterns. The values of partition coefficients used in our modeling are shown in Table B1.

[36] To take into account the temperature dependence of the clinopyroxene/melt partition coefficient we employed a procedure described by *Wood and Blundy* [1997]. The partition coefficients $D_{WB}(T)$ of *Wood and Blundy* [1997] were converted into a set of correction coefficients $\xi_{cpx/melt} = D_{WB}(T)/D_{WB}(T_{ref})$ related to a reference temperature T_{ref} = 1050°C, which may be regarded as a characteristic equilibration temperature for deformed high temperature mantle xenoliths [e.g., *Boyd et al.*, 1997]. The partition coefficients cpx/melt at any temperature can be found as the product of corresponding values from Table B1 and correction coefficients $\xi_{cpx/melt}$.

[37] To estimate the temperature dependence of garnet/melt partition coefficients we used the data of *Burgess and Harte* [2004] for eight rare earths (La, Ce, Nd, Sm, Eu, Dy, Er, Lu). However, *Burgess and Harte* [2004] calculated temperature dependence of the garnet/melt partition under the assumption of a constant cpx/melt partition coefficient. Thus the data of *Burgess and Harte* [2004] refer to gt/cpx rather than to gt/melt partition. The data of *Burgess and Harte* [2004] display a linear dependence log(D) vs $1/T$ (here T is the absolute temperature), in agreement with general theory [*McIntire*, 1963] and lattice strain model [*Blundy and Wood*, 1994]. To obtain a functional dependence on temperature for all rare earths we interpolated the data of *Burgess and Harte* [2004] linearly over the inverse temperature ($1/T$), as well as between the elements. By relating the calculated values to the reference temperature of T_{ref} = 1050°C, we obtained a set of correction coefficients $\xi_{gt/cpx}$. The temperature correction to partition coefficients gt/melt was then defined as $\xi_{gt/melt} = \xi_{gt/cpx}\xi_{cpx/melt}$. The correction coefficients used in this paper are shown in Figures B1 and B2.

Acknowledgments

[38] We thank Ed Stolper and Dan McKenzie for a discussion. Ed Stolper has provided extensive and thoughtful comments on an early version of this manuscript which are greatly appreciated. We gratefully acknowledge reviews by Sven Maaløe and Oded Navon, and the recommendations of the Associate Editor Roberta Rudnick, which helped us to clarify the main issues of the paper. This work was supported by NSF (grants EAR-0208165 and 0450035). Data and numerical codes used in this study are available from the authors.

References

Aharonov, E., P. Whitehead, P. Kelemen, and M. Spiegelman (1995), Channeling instability of upwelling melt in the mantle, *J. Geophys. Res.*, *100*, 20,433–20,450.

Blundy, J., and B. Wood (1994), Prediction of crystal-melt partition coefficients from elastic moduli, *Nature*, *372*, 452–454.

Boyd, F., N. Pokhilenko, D. Pearson, S. Mertzman, N. Sobolev, and L. Finger (1997), Composition of the Siberian cratonic mantle: Evidence from Udachnaya peridotite xenoliths, *Contrib. Mineral. Petrol.*, *128*, 228–246.

Boyd, F., K. Pearson, D. G. Hoal, B. Hoal, P. Nixon, M. Kingston, and S. Mertzman (2004), Garnet lherzolites from Louwrensia, Namibia: Bulk composition and P/T relations, *Lithos*, *77*, 573–592.

Burgess, S., and B. Harte (2004), Tracing lithosphere evolution through the analysis of heterogeneous G9-G10 garnets in peridotite xenoliths, II: REE chemistry, *J. Petrol.*, *45*, 609–644.

Chalapathi Rao, N., S. Gibson, D. Pyle, and A. Dickin (2004), Petrogenesis of proterozoic lamproites and kimberlites from the Cuddapah basin and Dharwar craton, southern India, *J. Petrol.*, *45*, 907–948.

Connolly, J., and Y. Podladchikov (1998), Compaction-driven fluid flow in viscoelastic rock, *Geodin. Acta*, *11*, 55–84.

Cox, K., J. Gurney, and B. Harte (1973), Xenoliths from the Matsoku pipe, in *Lesotho Kimberlites*, edited by P. Nixon, pp. 76–100, Lesotho Nat. Dev. Corp., Cape Town, South Africa.

Crough, S., W. Morgan, and R. Hargraves (1981), Kimberlites: Their relation to mantle hotspots, *Earth Planet. Sci. Lett.*, *50*, 260–274.

Dawson, J. (1971), Adwances in kimberlite geology, *Earth Sci. Rev.*, *7*, 187–214.

Dawson, J. (1980), *Kimberlites and Their Xenoliths*, Springer, New York.

Dawson, J. (2002), Metasomatism and partial melting in upper mantle peridotite xenoliths from the Lashaine volcano, Northern Tanzania, *J. Petrol.*, *43*, 1749–1777.

Eggler, D. (1989), Kimberlites: How do they form?, in *Kimberlite and Related Rocks*, vol. 1, *Their Composition, Occurrence, Origin and Emplacement*, edited by J. Ross et al., pp. 489–504, Blackwell Sci., Malden, Mass.

Eggler, D., and R. Wendlandt (1979), Experimental studies on the relationship between kimberlite magmas and partial melting of peridotite, in *Kimberlites, Diatremes, and Diamonds: Their Geology, Petrology, and Geochemistry*, vol. 1, edited by F. Boyd and H. Meyer, pp. 330–338, AGU, Washington, D. C.

Erlank, A., F. Waters, S. Hawkesworth, C. J. Haggerty, H. Allsop, R. Rickard, and M. Menzies (1987), Evidence for mantle metasomatism in periotitic nodules from the Kimberley pipes, South Africa, in *Mantle Metasomatism*, edited by M. Menzies and C. Hawkesworth, pp. 221–309, Elsevier, New York.

Faul, U. (1997), Permeability of partially molten rocks from experiments and percolation theory, *J. Geophys. Res.*, *102*, 10,299–10,311.

Fialko, Y. A., and A. M. Rubin (1999), Thermal and mechanical aspects of magma emplacement in giant dike swarms, *J. Geophys. Res.*, *104*, 23,033–23,049.

Golubeva, Y., I. Ilupin, and D. Zhuravlev (2003), Rare earth elements in kimberlites of Yakutia: Evidence from ICP-MS data, *Dokl. Earth Sci.*, *391*, 693–696.

Grégoire, M., B. Moine, S. O'Reilly, J. Cottin, and A. Giret (2000), Trace element residence and partitioning in mantle xenoliths metasomatized by highly alkaline, silicate- and carbonate-rich melts (Kerguelen Islands, Indian ocean), *J. Petrol.*, *41*, 477–509.

Grégoire, M., D. Bell, and A. le Roex (2003), Garnet lherzolites from the Kaapvaal craton (South Africa: Trace element evidence for a metasomatic history, *J. Petrol.*, *44*, 629–657.

Harte, B. (1987), Metasomatic events recorded in mantle xenoliths: An overview, in *Mantle Xenoliths*, edited by P. Nixon, pp. 625–640, John Wiley, Hoboken, N. J.

Harte, B., and M. Kirkley (1997), Partitioning of trace elements between clinopyroxene and garnet: Data from mantle eclogites, *Chem. Geol.*, *136*, 1–24.

Harte, B., R. Hunter, and P. Kinny (1993), Melt geometry, movement and crystallization, in relation to mantle dykes, veins and metasomatism, *Philos. Trans. R. Soc. London, Ser. A*, *342*, 1–21.

Heaman, L., B. Kjarsgaard, and R. Creaser (2003a), The timing of kimberlite magmatism in North America: Implications for global kimberlite genesis and diamond exploration, *Lithos*, *71*, 153–184.

Heaman, L., B. Kjarsgaard, and R. Creaser (2003b), The temporal evolution of North American kimberlites, *Lithos*, *76*, 377–397.

Hofmann, A. (1972), Chromatographic theory of infiltration metasomatism and its application to feldspars, *Am. J. Sci.*, *272*, 69–90.

Ionov, D., J. Bodinier, S. Mukasa, and A. Zanetti (2002a), Mechanisms and sources of mantle metasomatism: Major and trace element compositions of peridotite xenoliths from Spitsbergen in the context of numerical modelling, *J. Petrol.*, *43*, 2219–2259.

Ionov, D., S. Mukasa, and J. Bodinier (2002b), Sr-Nd-Pb isotopic compositions of peridotite xenoliths from Spitsbergen: Numerical modelling indicates Sr-Nd decoupling in the mantle by melt percolation metasomatism, *J. Petrol.*, *43*, 2261–2278.

Kelemen, P. B., G. Hirth, N. Shimizu, M. Spiegelman, and H. Dick (1997), A review of melt migration processes in the adiabatically upwelling mantle beneath oceanic spreding ridges, *Philos. Trans. R. Soc. London, Ser. A*, *355*, 283–318.

Kesson, S., A. Ringwood, and W. Hibberson (1992), Kimberlite melting relations revisited, *Earth Planet. Sci. Lett.*, *121*, 261–262.

Kohlstedt, D., Q. Bai, Z. Wang, and S. Mei (2000), The grain scale distributiion of silicate, carbonate and metallosulfide partial melts: A review of theory and experiments, in *Physics and Chemistry of Partially Molten Rocks*, edited by N. Bagdassarov, D. Laporte, and A. Thompson, pp. 3–28, Springer, New York.

Kopylova, M., and G. Garo (2004), Mantle xenoliths from southeastern Slave craton: Evidence for chemical zonation in thick, cold lithosphere, *J. Petrol.*, *45*, 1045–1067.

Korzhinskii, D. (1970), *Theory of Metasomatic Zoning*, 162 pp., Clarendon, Oxford, UK.

Laporte, D., and A. Provost (2000), The grain scale distributiion of silicate, carbonate and metallosulfide partial melts: A review of theory and experiments, in *Physics and Chemistry of Partially Molten Rocks*, edited by N. Bagdassarov, D. Laporte, and A. Thompson, pp. 93–140, Springer, New York.

le Roex, A., D. Bell, and P. Davis (2003), Petrogenesis of Group I kimberlites from Kimberley, South Africa: Evidence from bulk-rock geochemistry, *J. Petrol.*, *44*, 2261–2286.

Liang, Y., J. Price, D. Wark, and E. Watson (2001), Nonlinear pressure diffusion in a porous medium: Approximate solutions with applications to permeability measurements using transient pulse decay method, *J. Geophys. Res.*, *106*, 529–536.

Lister, J. R., and R. C. Kerr (1991), Fluid-mechanical models of crack propagation and their application to magma transport in dykes, *J. Geophys. Res.*, *96*, 10,049–10,077.

Maaløe, S. (1995), Geochemical aspects of primary magma accumulation from extended source regions, *Geochim. Cosmochim. Acta*, *59*, 5091–5101.

McDonough, W., and S.-s. Sun (1995), The composition of the Earth, *Chem. Geol.*, *120*, 223–253.

McIntire, W. (1963), Trace element partition coefficients—A review of theory and applications to geology, *Geochim. Cosmochim. Acta*, *27*, 1209–1264.

McKenzie, D. (1985), The extraction of magma from the crust and mantle, *Earth Planet. Sci. Lett.*, *74*, 81–91.

McKenzie, D. (1989), Some remarks on the movement of small melt fractions in the mantle, *Earth Planet. Sci. Lett.*, *95*, 53–72.

McKenzie, D., and R. O'Nions (1991), Partial melt distributions from inversion of rare earth concentrations, *J. Petrol.*, *32*, 1021–1091.

Menzies, M., N. T. A. Rogers, and C. Hawkesworth (1987), Metasomatic and enrichment processes in lithospheric peridotites: An effect of asthenosphere-lithosphere interaction, in *Mantle Metasomatism*, edited by M. Menzies and C. Hawkesworth, pp. 313–361, Elsevier, New York.

Mitchell, R. (1986), *Kimberlites: Mineralogy, Geochemistry, and Petrology*, 442 pp., Springer, New York.

Mitchell, R. (1995), *Kimberlites, Orangeites, and Related Rocks*, 410 pp., Springer, New York.

Navon, O., and E. Stolper (1987), Geochemical consequences of melt percolation: The upper mantle as a chromatographic column, *J. Geol.*, *95*, 285–307.

Onuma, N., H. Higuchi, H. Wakita, and H. Nagasawa (1968), Trace element partition between two pyroxenes and the host lava, *Earth Planet. Sci. Lett.*, *5*, 47–51.

Ringwood, A., S. Kesson, W. Hibberson, and N. Ware (1992), Origin of kimberlites and related magmas, *Earth Planet. Sci. Lett.*, *113*, 521–538.

Rubin, A. (1998), Dike ascent in partially molten rock, *J. Geophys. Res.*, *103*, 20,901–20,919.

Saltzer, R., N. Chatterjee, and T. Grove (2001), The spatial distribution of garnets and pyroxenes in mantle peridotites: Pressure-temperature history of peridotites from the Kaapvaal craton, *J. Petrol.*, *42*, 2215–2229.

Schmidberger, S., and D. Francis (2001), Constraints on the trace element composition of the Archean mantle root beneath Somerset Island, Arctic Canada, *J. Petrol.*, *42*, 1095–1117.

Simon, N., G. Irvine, G. Davies, D. Pearson, and R. Carlson (2003), The origin of garnet and clinopyroxene in 'depleted' Kaapvaal peridotites, *Lithos*, *71*, 289–322.

Smith, D., and F. Boyd (1987), Compositional heterogeneities in a high temperature lherzolite nodule and implications for mantle processes, in *Mantle Xenoliths*, edited by P. Nixon, pp. 551–561, John Wiley, Hoboken, N. J.

Sobolev, N. (1977), *Deep Seated Inclusions in Kimberlites and the Problem of the Composition of the Upper Mantle*, AGU, Washington, D. C.

Spence, D., and D. Turcotte (1990), Buoyancy-driven magma fracture: A mechanism for ascent through the lithosphere and the emplacement of diamonds, *J. Geophys. Res.*, *95*, 5133–5139.

Spetsius, Z., and V. Serenko (1990), *Composition of the Continental Mantle and the Lower Crust Beneath the Siberian Platform* (in Russian), Nauka, Moscow.

Spiegelman, M., and P. B. Kelemen (2003), Extreme chemical variability as a consequence of channelized melt transport, *Geochem. Geophys. Geosyst.*, *4*(7), 1055, doi:10.1029/2002GC000336.

Tainton, K., and D. McKenzie (1994), The generation of kimberlites, lamproites, and their source rocks, *J. Petrol.*, *35*, 787–817.

Ukhanov, A., I. Ryabchikov, and A. Khar'kiv (1988), *The Lithospheric Mantle of the Yakutian Kimberlite Province* (in Russian), Nauka, Moscow.

van Orman, J., T. Grove, and N. Shimuzu (2001), Rare earth element diffusion in diopside: Influence of temperature pressure and ionic radius, and an elastic model for diffusion in silicates, *Contrib. Mineral. Petrol.*, *141*, 687–703.

van Westrenen, W., J. Blundy, and B. Wood (1999), Crystal-chemical controls on trace element partitioning between garnet and anhydrous silicate melt, *Am. Mineral.*, *84*, 838–847.

Vladimirov, B., L. Solovyeva, A. Kiselev, K. Yegorov, M. Maslovskaya, L. Dneprovskaya, S. Brandt, and V. Semenova (1990), *Kimberlites and Kimberlite-Like Rocks: Kimberlites as Ultramaphic Formation of Old Platforms* (in Russian), Nauka, Moscow.

Wark, D., and E. Watson (1998), Grain size permeabilities of texturally equilibrated monominerallic rocks, *Earth Planet. Sci. Lett.*, *164*, 591–605.

Wedepohl, K., and Y. Muramatsu (1979), The chemical composition of kimberlites compared with the average composition of three basaltic magma types, in *Kimberlites, Diatremes and Diamonds: Their Geology, Petrology and Geochemistry*, edited by F. Boyd and H. Meyer, pp. 300–312, AGU, Washington, D. C.

White, R., and D. McKenzie (1989), Magmatism in rift zones: The generation of volcanic continnental margins and flood basalts, *J. Geophys. Res.*, *94*, 7685–7729.

Wood, B., and J. Blundy (1997), A predictive model for rare element partitionig between clinopyroxene and anhydrous silicate melt, *Contrib. Mineral. Petrol.*, *129*, 166–181.

Wyllie, P. (1980), The origin of kimberlites, *J. Geophys. Res.*, *85*, 6902–6910.

Wyllie, P. (1995), Experimental petrology of upper mantle materials, processes and products, *J. Geodyn.*, *20*, 429–468.